



ENGINEER

JOURNAL OF THE INSTITUTION OF ENGINEERS, SRI LANKA

VOL: XXXXIII, NO: 03

July 2010

ISSN - 1800-1122



EDITORIAL BOARD

Eng. H D S de Alwis - President
Eng. D L O Mendis - Past President
Eng. L W Seneviratne - Chairman, LPP&C
Eng. (Prof.) T. M. Pallewatta - Editor "ENGINEER"
Editor, Annual Trans.
(Tech. Papers)

Eng. (Dr.) D A R Dolage
Eng. M Harsha Wickremasinghe
Eng. (Miss.) Arundathi Wimalasuriya - Ex. Secretary
Eng. M. L. Weerasinghe - Editor "SLEN"

The Institution of Engineers, Sri Lanka
120/15, Wijerama Mawatha,
Colombo - 00700
Sri Lanka.

Telephone: 94-11-2698426, 2685490, 2699210

Fax: 94-11-2699202

E-mail: iesl@slt.lk

E-mail (Publications): ed@sltnet.lk

Website: <http://www.iesl.lk>

The statements made or opinions expressed in the "Engineer" do not necessarily reflect the views of the Council or a Committee of the Institution of Engineers Sri Lanka, unless expressly stated.

COVER PAGE



The Magampura (Hambantota) port under construction. This port is unique in the sense that it is an inland harbour excavated in to the land, to be inundated by the sea after construction. This technique of port construction has its advantage that most of the construction works could be conducted under dry conditions. First stage of the harbour construction will be concluded with the initiation of the inundation process in August.

Courtesy of Eng. L. N. Perera & Sri Lanka Ports Authority

From the Editor ...

SECTION I

Kinematic and Inertial Effects of Earthquakes on Rock Socketed Single Piles in a Two-Layered Medium

by : Eng. (Dr.) H S Thilakasiri

Effects of Large Retarder Overdose on Concrete Strength Development

by : Eng. (Prof.) W P S Dias, M A N Sewapriya, E A C K Edirisooriya and C G Jayathunga

Correlation among Hydraulic Parameters of Moving Hydraulic Jump in Rectangular Open Channels

by : M C M Nasvi, Z A M Asmeer, F M Mowsoom and Eng. (Prof.) K P P Pathirana

Forecasting Thermal Stratification of the Victoria Reservoir using a Hydrodynamic Model

By : Eng. (Prof.) K D W Nandalal, Prof. S Piyasiri and K G A M C S Abeysinghe

An Approach to Grade Aggregate having Mild Potential Alkali-Silica Reactivity

by : Eng. C K Pathirana, Eng. H Abeyruwan, Dr. H M G T A Pitawal and Eng. (Dr.) A P N Somaratna

Suitable Bridge Pier Section for a Bridge over a Natural River

by : Eng. G A P Gampathi

SECTION II

Trial Introduction of a Bus Lane on A02 : A Post -Mortem

by : Eng. (Prof.) K S Weerasekera

Computer Aided Design of Modern High-Rise Building

by : Eng. G A P Gampathi and Eng. P P P Peiris



FROM THE EDITOR.....

Magampura or in other words Hambantota Port development project is one of the mega construction works undertaken by our country. In fact, it is the largest project to progress after the country was liberated from the clutches of terrorism. Though Sri Lanka does not have the land space to spare, the concept of this inland harbour is technically as well as economically favourable since almost all construction work could be handled under dry conditions.

It is needless to say that the major professional steering any such infrastructure project is the Engineer. From inception to completion and even beyond completion, an infrastructure project requires engineering inputs at all levels. In whatever scale one feels to perceive, successful completion of such a development project would make the players involved, especially the Engineers, feel proud and accomplished. It is achievements such as these that we could show with pride to our grand children.

However, the level of pride and accomplishment derived by us, the Engineers of Sri Lanka, is directly proportional to our positive involvement. We should look back and see whether it had been adequate and if we see that it is not, the only recourse would be to increase it by being confident, assertive and proactive. After all, who could be more conscientious about the future of our country than us?

Eng. (Prof.) T. M. Pallewatta, Int. PEng (SL), C. Eng, FIE (SL), FIAE(SL)

Editor, 'ENGINEER', Journal of The Institution of Engineers.

Editor, Technical Papers for the Transactions of The Institution of Engineers.



SECTION I



Kinematic and Inertial Effects of Earthquakes on Rock Socketed Single Piles in a Two-Layered Medium

H. S. Thilakasiri

Abstract: The behaviour of piles in a two-layered soil medium subjected to earthquake ground accelerations are investigated using finite element method. The kinematic and inertial effects on rock socketed piles in a two-layered soil medium are investigated in this study considering the soil properties relevant to Sri Lanka. Hyperbolic nonlinear constitutive model is used for modelling the behaviour of the fully coupled soil medium. The effect of the earthquake was simulated by lateral ground acceleration applied to the bedrock and in this respect two earthquake records measured at a considerable distance away from the epicentre are used in the numerical simulation to take into account large epicentral distance to an anticipated earthquake that might affect Sri Lanka. The validity of the results of the proposed model was established by comparing with the trends observed in similar studies reported in the literature. A detailed parametric study of the kinematic bending moments developed in piles at the layer interface of the two-layered medium is carried out using the developed model. Furthermore, the effects of the inertial forces on the kinematic bending moment developed at the layer interfaces are investigated by varying the pile diameter and the effective masses at the pile head. Moreover, the variation of the bending moments, developed in the pile due to the combined effects of the kinematic and inertial responses of the pile-soil system, with the effective mass at the pile head for different pile diameters is also investigated.

Keywords: Rock socketed bored piles, earthquake, layered mediums, inertial forces

1.0 Introduction

Earthquakes are generally confined to certain zones in the world and these zones are concentrated along the active plate boundaries of the earth's crust. Fortunately, Sri Lanka is situated well away from the plate boundaries and it is believed that Sri Lanka is safer from the devastating effects of earthquakes. This is true to some extent but one should not be complacent and completely disregards the effects of earthquakes in the design of structures in Sri Lanka. There are few reasons for considering effects of a certain magnitude earthquake in designing structures in Sri Lanka:

- Some minor tremors are already felt in some parts of the country;
- During the design life of a structure possibility of experiencing a certain magnitude ground motion;
- Possibility of transmitting ground vibrations from a far away earthquake through the bedrock and affecting especially the structures on piles socketed to the bedrock; and
- The minor nature of the additional measures required to guard the structures against the effects of smaller magnitude earthquakes.

It is very important that engineers responsible for the design takes certain measures to safe guard the structures against the effects of a possible ground motion. Such ground motions, if ever happens, may have devastating effects on structures which are designed and constructed without considering the effects of such ground motion. However, one should not take this statement out of context and design the structures considering large magnitude earthquakes. The institutions responsible for developing design and construction guidelines in Sri Lanka should also take some meaningful actions to incorporate the effects of appropriate magnitude ground motion in the design and construction standards.

Experimental and theoretical research works related to dynamic forces on pile foundations due to ground motion are carried out especially in countries affected by earthquakes. There are large number of theoretical studies carried out to investigate the behaviour of single pile and pile groups in homogeneous soil mediums (Novak, 1991, Kuhlemeyer, 1979 and, Makris and Gazetas, 1992) by making varying

Eng. (Dr.) H. S. Thilakasiri, C. Eng., PEng(SL), FIE(Sri Lanka), B.Sc. Eng. (Hons) (Moratuwa), M.Sc. (Lond), DIC, PhD(USF), Senior Lecturer, Department of Civil Engineering, University of Moratuwa, Sri Lanka.



assumptions regarding the excitation ground motion and idealization of the soil medium.

Other theoretical simulation researches (Gazetas and Mylonakis, 1998, and Gazetas and Dobrej, 1984) were also carried out to investigate the behaviour of piles in layered soil medium subjected to lateral ground motion. However, none of these researches were conducted considering the nonlinear coupled behaviour of the soil medium and the random nature of the natural earthquake excitations. Moreover, no research work is carried out considering the subsurface conditions and typical foundations in Sri Lanka to investigate the effects of a possible ground motion on local structures. Without the guidance from such research work, it is very difficult to improve the earthquake resistance of the foundations in Sri Lanka. Therefore, with that objective in mind a research programme was initiated to investigate the effects of earthquakes on rock socketed pile foundations in Sri Lanka.

Thilakasiri et al. (2009) presented kinematic effects of earthquakes on piles in layered soil mediums in Sri Lanka based on a numerical simulation using finite element method. This paper further investigates the development of kinematic forces in single piles and strengthens the findings presented in Thilakasiri et al. (2009). In addition, this paper also presents the results of the numerical simulation work carried out to investigate the combined effects of kinematic and inertial forces. It should be noted here that the behaviour of pile groups may be different from the behaviour of single piles due to the interaction between the piles in a group and should be considered separately.

1.1 Effects of Earthquakes on Pile Foundations in a layered soil medium

As previously mentioned, there is a possibility of transmitting the ground motion due to earthquakes along the basement rock to other regions of the earth crust well away from the epicenter. As a result, there is a possibility that the rock socketed end bearing bored piles may be subjected to the effects of such earthquakes due to the movement of the bedrock. Therefore, rock socketed bored piles, widely used in Sri Lanka, are considered in the present investigation. In most locations in Sri Lanka, soft alluvial soil deposits are present above the hard residual formations. Due to the above mentioned reasons, a pile socketed to the bedrock in a two layer soil medium with a soft

alluvial deposit overlying a hard residual formation is considered in the present study.

A pile supporting a structure is subjected to two types of earthquake induced forces: *Inertial forces*; and *Kinematic forces*. In simple terms the inertial forces are developed due to the mass on the pile head and the kinematic forces are developed due to the difference of the rigidity of the surrounding soil medium and that of the pile.

It is typically found that when a structure is supported on a pile, the motion of the pile is transferred to the structure and the structure is forced to oscillate. The oscillatory motion of the mass of the structure generates inertial forces that in turn is applied on the pile and hence on the soil. The deformation of the pile due to the inertial forces may further change the inertial forces in the superstructure. This is referred to as the *inertial response*.

Generally the effects of the inertial forces are concentrated within very shallow depths (less than about ten times the pile diameter below the ground surface). However, Mizuno (1978) observed failures of piles at depths below the levels generally attributed to inertial effects. After similar other observations, the research work was focused to find the cause of such failures. Based on the evidence of numerical and experimental studies, such failures were attributed to discontinuities in the subsurface due to sudden variations in the soil stiffness and such effects were termed as *kinematic effects* of the earthquake on piles. Furthermore, some research work using centrifugal model tests (Boulanger et al., 1999) using soft clay layer overlying a dense sand layer showed an increase in the peak bending moment near the interface between the two layers. A brief description of the way kinematic forces are developed in a pile embedded in a layered medium is given below.

The soil response at a given site without any structural element is referred to as the 'free field' motion of the site. Due to the variations of the stiffness of the soil layers, the lateral motion of the layers due to the horizontal ground acceleration created by the earthquake may considerably vary. Now consider a pile embedded in a layered soil medium. Due to the high inertial effects of the surrounding soil, the pile is forced to follow the movement of the surrounding soil medium. However, due its high rigidity the piles resist such forced

movement and reflect the incident stress waves in the process. This is referred to as the wave scattering and as a result, the ground motion near the pile considerably differs from the free field motion.

As a result of this forced oscillation, the pile may develop curvature and hence, the development of bending moments and shear forces in the pile. This is referred to as the *kinematic response* of the pile. When the pile is in a layered soil medium, the curvature near the layer interface may be higher as the difference in displacement pattern of the layers due to the non-uniform stiffness of the adjacent layers. The magnitudes of such kinematic forces, developed in piles, mainly depend on the contrast between the layers in the subsurface and have maximum effects near the boundaries between the layers in the subsurface (Gazetas and Mylonakis, 1998).

The present codes of practice take into account only the inertial forces. There are mainly two calculation procedures used in most of the design codes. For example Indian code of practice for design seismic forces for buildings, elevated liquid storage tanks, stacks, concrete and masonry dams, embankments, bridges, and retaining walls (IS:1893, 1984) specifies the use of two procedures for the estimation of lateral forces on buildings:

- i. Seismic Coefficient method; and
- ii. Response Spectrum Method.

For the use of the code provisions, India is divided into five seismic zones I to V with the associated Modified Mercalli Intensity (MMI) V (or less), VI, VII, VIII, and (IX (and above) respectively. In seismic coefficient and response spectrum methods, due consideration is given to the seismic zone where the structure is located, importance of the structure, soil-foundation system, ductility of constructions, flexibility of the structure, and weight of the building. The estimated lateral force is applied as a static base shear force on the piles and the bending moments and shear forces generated in the pile are estimated. It is proved that the dynamic loading due to the superstructure inertial effects in piles is confined to a shallow length, termed active length, below the ground surface.

The bending moment developed in a 1.2m diameter 20m long pile, supporting a five storey office building with a plan area of 50m x 50m, is estimated assuming the conditions relevant to Zone II in India. It is assumed that the pile is loaded to an axial stress equivalent to 5000 kPa and the seismic coefficient method is used to estimate the lateral force on the pile.

Then, the bending moment developed in the pile is estimated using the theory of laterally loaded piles and the developed bending moment diagram is shown in Figure 1.

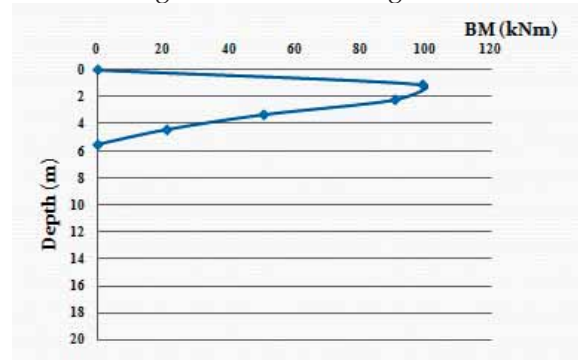


Figure 1 – Bending moment diagram of a 1.2m diameter 20m long pile due to inertial effects.

It is clear from the above discussion that the inertial forces for a given earthquake excitation depend on the effective mass oscillating with the pile at the pile head. The effective mass relevant to a pile head depends on many factors such as the mass of the superstructure, distribution of the mass within the superstructure and the stiffness of different elements of the structure. On the other hand, the magnitude of the kinematic forces for a given earthquake excitation depends on the rigidity of the pile, stiffness and the variation of the stiffness of the surrounding soil medium along the pile shaft. Even though the total forces on the pile is the summation of the inertial and the kinematic forces, the relative magnitude of the individual component depends on many factors as mentioned above. Therefore, it is very important that for design purposes the effects of both the components be considered to take into account the total forces developed in the pile.

In this study, it is intended to investigate the combined effects of both the kinematic and inertial effects on a single rock socketed pile in a layered nonlinear two-phase soil medium. Considering the economy and the feasibility, numerical simulation with finite element method is used for the present investigation.

2.0 Investigation Methodology

2.1 Introduction

Finite Element Computer software, named Imperial College Finite Element Program (ICFEP), developed at the Soil Mechanics section of the Department of Civil and Environmental Engineering at Imperial College,



London, UK is used for the present study. ICFEP is specially developed to solve problems related to geotechnical engineering and has been successfully utilized for solving large number of complex geotechnical engineering problems. ICFEP possesses the capability of solving problems related to soil dynamics with the availability of suitable soil constitutive models and the capability of the applying dynamic boundary conditions (Kontoe, 2006).

2.2 Soil Constitutive Relationship

The ability of the soil constitutive relationship to model the accurate behaviour of the soil under dynamic loading is a major factor affecting the accuracy of any finite element model used in soil dynamics. For dynamic shearing problems, loading and unloading occur simultaneously. Since the soil does not behave elastically, the unloading and reloading paths do not generally follow the previous loading paths giving rise to hysteretic behaviour of soil. Hyperbolic nonlinear constitutive model is capable of numerically simulating this soil behaviour, when subjected to dynamic forces. In addition, it has the added advantage of well established correlations between the simple soil parameters and the damping ratio curves and stiffness decay curves (Guerreiro, 2008). According to the hyperbolic nonlinear constitutive model, the variation of the shear stress (τ) vs. shear strain(γ) of a soil element is shown in Figure 2.

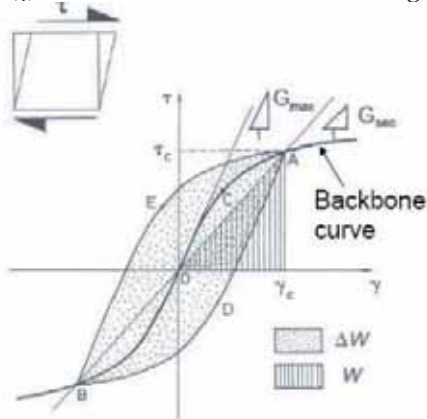


Figure 2 – Monotonic loading curve and hysteresis loop of hyperbolic nonlinear constitutive relationship during cyclic shearing.

In the present model, hyperbolic nonlinear constitutive model is used for the soil with the empirical correlation proposed by Darendali (2001). Material damping represents the energy dissipation due to several mechanisms such as internal friction, plastic deformation and heat

generation. The relevance of each mechanism changes with the strain amplitude. Area under the curve, ΔW in Figure 2, represents the energy dissipation due to material damping. Material damping ratio ξ is expressed as the ratio between the dissipated energy of the hysteresis loop (ΔW) and the stored elastic energy (W) as shown in Figure 2. The damping ratio is expressed by $\xi = (\Delta W / (4\pi W))$. The damping ratio of the soil vs. shear strain for the soil in Layer 1 of the developed model is shown in Figure 3.

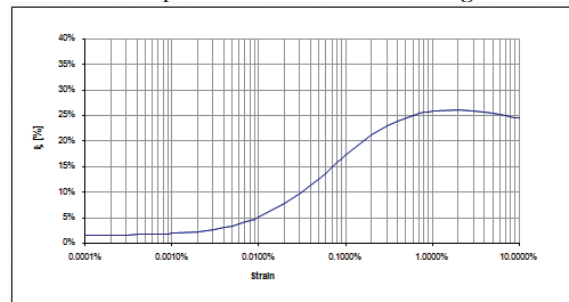


Figure 3 – Material damping ratio for soil in Layer 1 of the model.

2.3 Pile-Soil Model

A relatively soft alluvial deposit overlying a hard residual formation, typically found in most of the piling sites in Sri Lanka, is considered in the numerical simulation, as shown in Figure 4.

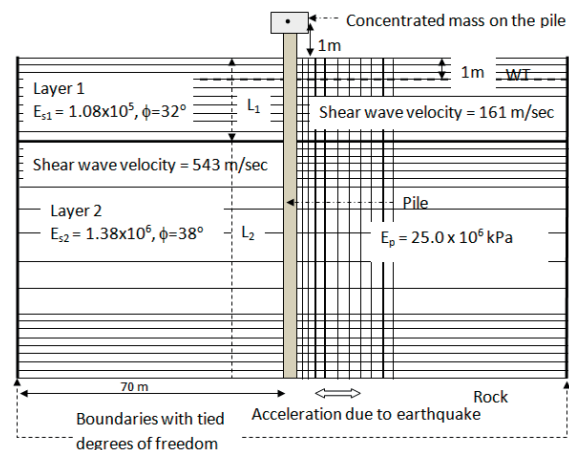


Figure 4 – Finite element model representing the pile-soil system.

The thickness of the top layer is taken as 5m and 8m while the overall thickness of the subsurface soil is kept constant at 20m. The initial elastic modulus, angle of internal friction, Poisson ratio of the top layer (Layer 1) are assumed to be 1.08×10^5 kN/m², 32° and 0.2 respectively while the same properties of the bottom layer (Layer 2) soil are assumed to be 1.38×10^6 kN/m², 38° and 0.2 respectively. The water table is located at 1m below the ground surface and initial hydrostatic pressure distribution is assumed.

Even though the behaviour of a pile is best modelled under three dimensional strain, considering the economy of the solution process plane strain condition was assumed in the model. The pile diameter is varied from 1200mm to 600mm and assumed to behave in a linear elastic manner with an elastic modulus of 25×10^6 kPa and Poisson ratio of 0.2. Only for the study of the inertial effects, the effective mass of the structure is considered by placing a mass equivalent to a certain percentage of the design load at a height of 1m above the ground surface, as shown in Figure 4.

In the present study, two horizontal ground acceleration records, shown in Figures 5 and 6, were used to get the ground excitation for the numerical simulation. It is assumed that the pile-soil system is subjected to ground acceleration only in one direction at a given time. Both the horizontal ground acceleration records considered in this study were measured more than about 200 km away from the epicentre, to take into the effects of large epicentral distance to Sri Lanka from an anticipated earthquake. The predominant frequency of the selected earthquake records are well away from the resonance frequency of the soil medium. This was done purposely as the kinematic effects on the pile are predominant under such conditions. Further, the maximum peak ground acceleration of both the earthquake records are less than 0.05g as an anticipated earthquake may be of low magnitude.

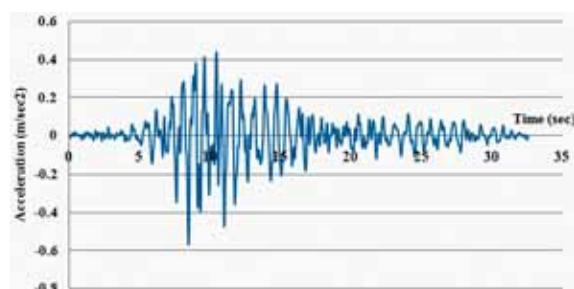


Figure 5 – Earthquake record 1.

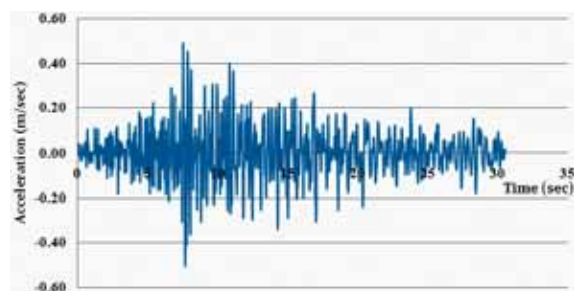


Figure 6 – Earthquake record 2.

Zienkiewicz et al. (1988) introduced a boundary condition, in which the degrees of freedom at

the lateral boundaries are tied. Thus the boundary nodes at the same elevation move in an identical fashion. This method can perfectly model the one dimensional soil response but it cannot absorb any waves radiating away from the structural element resulting wave trapping inside the mesh. Kontoe (2004) observed that the tied degrees of freedom boundary conditions at the mesh boundaries are suitable when the wave radiating away from the structure is negligible. Since there is no measure of the amount of wave radiating away from the pile, the boundary response of the pile soil system with tied degrees of freedom were compared with the response of the corresponding positions of the system without the pile ('free field' motion) subjected to the same excitation ground motion. The difference between the two systems was brought to acceptable limits by increasing the distance from the pile to the lateral boundary. In this case the material damping of the cyclic soil constitutive behaviour attenuates the wave so that the wave reflected at the boundary becomes insignificant.

Potts and Zdravkovic et al. (1988) showed that the results of finite element simulation depend on how the behaviour of the boundaries between different mediums are modelled. In this regards, the modelling of the interface between the pile modelled, with linear elastic material properties, and the surrounding soil, modelled with hyperbolic nonlinear constitutive relationship, is extremely important. The pile-soil interface was modelled with Mohr-Coulomb elasto-plastic behaviour with normal and shear stiffness. The normal and shear stiffness of the pile-soil interface elements are selected based on a sensitivity analysis of the maximum bending moment developed in the pile for different pile-soil interface shear and normal stiffness. The variation of the maximum bending moment developed in a fixed head pile for different pile-soil interface stiffness values for the top layer thicknesses 5m and 8m are shown in Figures 7 and 8.



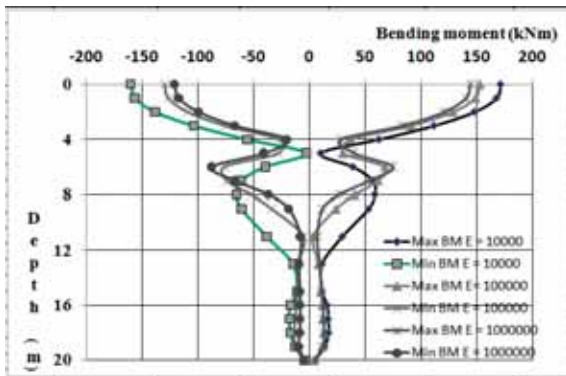


Figure 7 – Variation of the maximum and minimum BM with the pile-soil interface stiffness for top layer thickness 5m.

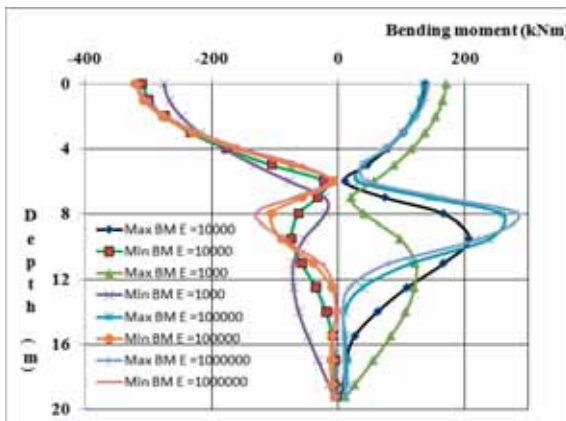


Figure 8 – Variation of the maximum and minimum BM with the pile-soil interface stiffness for top layer thickness 8m.

It is evident from the maximum bending moment variations shown in Figures 7 and 8 that the bending moment profiles does not vary significantly as the pile-soil interface stiffness is varied from 10^5 to 10^6 . Therefore, based on the results of the sensitivity analysis, the interface stiffness of 10^5 is used in the present study as shown in Potts and Zdravkovic et al. (1988). Furthermore, the mesh configuration and the size were selected based on the results of a sensitivity analysis of the results with respect to different mesh configurations.

3.0 Results of the Numerical Simulation

Thilakasiri et al. (2009) presented the results of a similar analysis carried out to investigate the kinematic forces developed in single pile socketed to bedrock. Thilakasiri et al. (2009) used the earthquake effects given by the horizontal ground acceleration shown in Figure 5. Based on the results of that analysis, it was concluded that:

- i. Basic trends observed by other experimental and simplified theoretical studies are observed;
- ii. Significant bending moment is developed in the pile near the layer interface;
- iii. The active length, L_a given by Equation [1], proposed by Gazetas and Mylonakis (1998) based on their study assuming linear elastic soil medium, is an important parameter in determining the behaviour of a pile in a two layer soil medium.

$$L_a = 1.5d \left(\frac{E_p}{E_{s1}} \right)^{0.25} \quad [1]$$

Where

- d - Pile diameter
- E_p - Elastic modulus of the pile material
- E_{s1} - Initial elastic modulus of the top layer

- iv. The stiffness decay of the soil layers increases the actual active length more than the active length estimated assuming initial elastic modulus of the top layer as given in Equation [1];
- v. The kinematic bending moment developed near the layer interface increases with the diameter of the pile;
- vi. The fixity at the pile head increases the bending moment at the pile head and slightly reduces the bending moment in the pile near the layer interface;
- vii. The BM at the pile top and at the interface for the fixed head condition are significantly different when the top layer thickness is less than the active length;
- viii. If the bottom layer is below the active length, its stiffness does not have a significant effect on the kinematic force developed in the pile;
- ix. A defect present near the layer interface reduces the kinematic bending moment developed. However, even with a defect near the layer interface, a kinematic bending moment of significant magnitude is developed.

3.1 Results of the Present Analysis

A fully coupled finite element simulation is carried out by first applying the working load on the pile and subsequently applying the horizontal ground acceleration to the bedrock. Figure 9 shows the shear stress vs. shear strain

behaviour of an element close to the pile during initial axial loading and subsequent shearing.

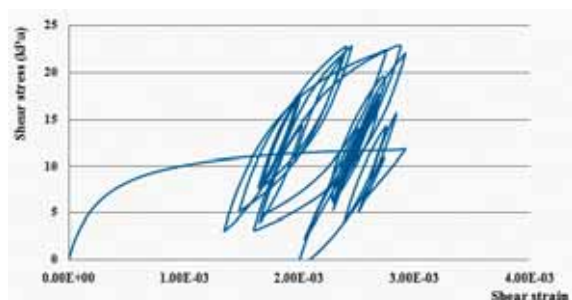


Figure 9 – Shear stress vs. shear strain of a soil element close to the pile during axial loading of the pile and lateral movement due to the earthquake.

The force developed at any level in the pile with an engineering significance is commonly considered to be the maximum bending moment developed at that level. Generally, the maximum bending moment along the entire pile shaft occurs when the relative horizontal displacement in the pile shaft is the maximum. Therefore, following the published research of similar studies, the maximum bending moment developed at each section during the ground motion is presented in this paper.

3.1.1 Kinematic Bending Moment

The maximum kinematic bending moments developed in the pile are further studied in the present paper to strengthen the findings of Thilakasiri et al. (2009) and to investigate the accuracy of the model developed by comparing with the already observed trends reported in the literature.

The variation of the maximum bending moment near the layer interface with different pile diameters are determined for the top layer thickness of 5m, as shown in Figure 10. Figure 11 shows the variations of the maximum bending moment developed at the pile top and at the layer interface for the active lengths of different pile diameters. It should be noted here that the active length is estimated from Equation [1] using the initial elastic modulus of the top layer soil.

The general trend observed from previous studies using linear elastic soil properties is that when the active length is more than the top layer thickness, the bending moment developed in the pile at the soil layer interface is less than the bending moment developed at the pile top. This trend is observed in Figure 11. However, it is interesting to note in Figure 11 that the pile top bending moment becomes greater than the

interface bending moment even when the active length, estimated using the initial elastic modulus of the soil, is less than the top layer thickness (5m). The reason for this is the stiffness degradation of the soil with the shear strain. Therefore, the effective elastic modulus is smaller than the initial elastic modulus of the soil and hence, the actual effective length may be higher than the effective lengths shown in Figure 11. This observation is very much in agreement with the findings of the Gazetas and Mylonakis (1998) using linear elastic soil medium.

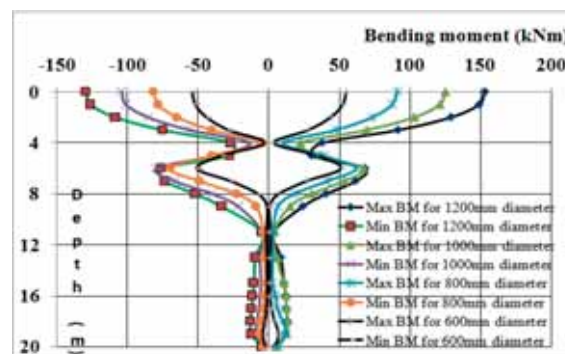


Figure 10 – Variation of the maximum and minimum bending moments along the pile shaft for different diameter piles with top layer thickness 5m.

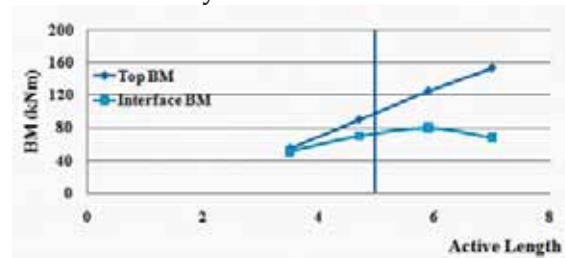


Figure 11 – Bending moment at the interface and top of the pile for fix-headed piles of different diameter in a soil medium with top layer thickness of 5m.

A different earthquake record is used to check the validity of the findings of Thilakasiri et al. (2009). For this purpose, earthquake ground acceleration record 2 given in Figure 6 is used with the top layer thickness of 8m. The obtained maximum and minimum bending moments along the pile shaft are shown in Figure 12. Figure 13 shows the variations of the pile top bending moment and the bending moment developed at the layer interface with the active length of the piles.

Similar to the Figure 11, the pile top bending moment becomes greater than the interface bending moment for active lengths less than the top layer thickness. The reason for such deviation is the degradation of the elastic



modulus with the shear strain as explained earlier. Therefore, this may be taken as a further verification of the developed model.

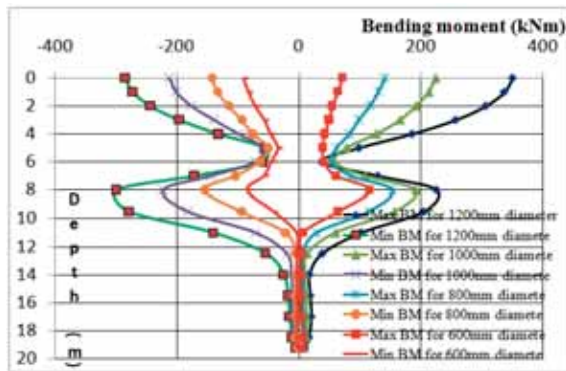


Figure 12 – Variation of the maximum and minimum bending moments along the pile shaft, obtained for the acceleration record 2, for different diameter piles with top layer thickness 8m.

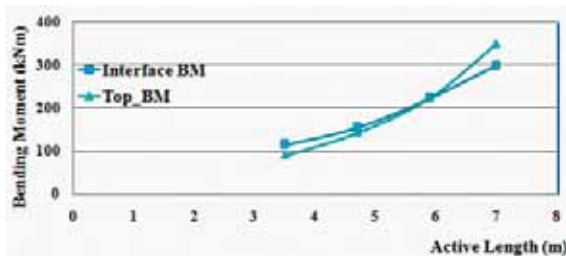


Figure 13 – Bending moment at the interface and top of the pile, obtained from acceleration record 2, for fix-headed different diameter piles in a soil medium with top layer thickness of 8m.

The above findings are very much in agreement with the general trends that were observed in similar analysis. Therefore, based on the above findings one could conclude that the results obtained from the model is reasonably accurate. However, a true verification of model predictions may be confirmed only by comparing with the field or laboratory measured forces developed in piles subjected to earthquake ground motion. The findings of this study are in excellent agreement with the previous observations made by Thilakasiri et al. (2009). Therefore, the findings of the present study strengthen the conclusions made by Thilakasiri et al. (2009) related to the kinematic forces developed in piles subjected to earthquake ground motion.

3.1.2 Combined effects of Inertial and Kinematic Effects

The main aim of this study is to investigate the combined effects of the inertial and kinematic forces on a single rock socketed pile. To simulate the mass of the structure on the pile, a weight was kept on the pile at 1m above the ground surface. The weight that was kept on the pile was varied to one-tenth of the working load and one-fourth of the working load. A certain mass of the structure may be directly on the pile and may oscillate with the pile. The mass that moves with a single degree of freedom assumed in this simulation may be relatively smaller in a structure such as a building consisting of distributed mass. In such cases only the mass of the pile cap, portion of the capping beam and the columns directly attached to the pile may contribute to the inertial effects on the pile. However, in short bridge piers the assumption of single degree of freedom system with a relatively high percentage of weight on the pile head may be realistic. Therefore, in such structures both the inertial and kinematic forces should be considered.

Figure 14 shows the maximum and minimum bending moments generated in a 1200mm diameter pile without mass, mass equivalent to one-tenth of the working load and one-fourth of the working load kept 1m above the pile head as shown in Figure 4.

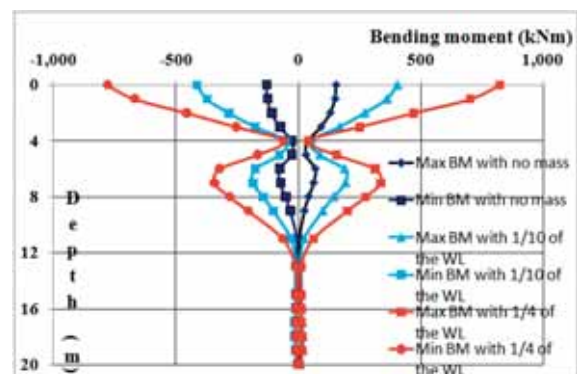


Figure 14 – Maximum and minimum BM in 1200mm diameter pile with different mass on the pile head for 5m thick top layer.

The developed bending moment in the pile clearly indicates that the interface bending moments are also increased with the mass on the pile head. However, the increase in the pile top bending moment takes place at a higher rate than the interface bending moment. It should be noted here that the active length of

the pile is more than the thickness of the top layer.

The maximum and minimum bending moments developed in different diameter piles with a mass equivalent to one-fourth of the design load and one-tenth of the design load placed at the pile head are shown in Figures 15 and 16 respectively.

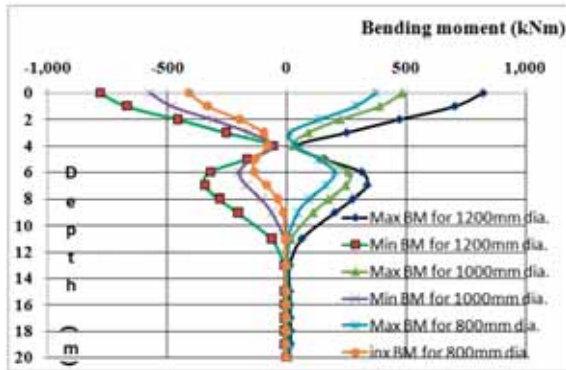


Figure 15 - Maximum and minimum BM with 1/4th of the working load on the pile head for different diameter piles for 5m thick top layer.

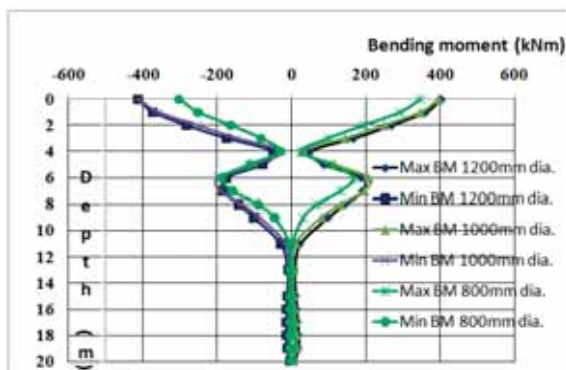


Figure 16 - Maximum and minimum BM with 1/10th the working load on the pile head for different diameter piles for 5m thick top layer.

The variation of the pile top and interface bending moments with the mass at the pile head for different pile diameters are shown in Figure 17.

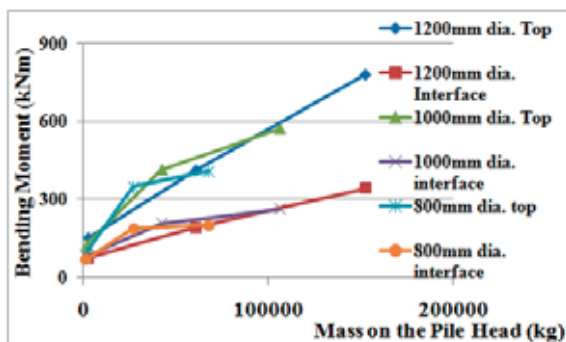


Figure 17 – Variation of the pile top and Interface BMs with the mass at the pile head for different pile diameters.

Both the pile top bending moment and the bending moment at the layer interface increases with the increase in the mass placed at the pile head. It seems that the pile top bending moment increase at a faster rate than the interface bending moment. Rate of increase in both the top and the interface bending moments seems to decrease with the increasing in the mass placed at the pile head.

The increase in the pile head bending moment with the mass on the pile head is clearly visible in Figure 17. However, the variation of the pile top and interface bending moment with the mass at the pile head should be investigated further to quantify the effects of different parameters on the variation of the bending moments. Damage to large number of flyover bridges during earthquakes may be due to the large effective mass oscillating with the head of the pier head and the resulting large bending moments developed in the bridge piers.

The interface bending moment developed due to the kinetic effects are increased due to the inertial effects of the effective mass at the pile head. Therefore, higher kinetic effects should be expected if the mass directly attached to the pile head is higher.

4.0 Conclusions

The importance of the active length in relation to the top layer thickness for the development of the bending moment in a pile subjected to earthquake effects is further verified by the present study. However, it is shown by the present study that the stiffness degradation of the soil with the shear strain should be considered in the estimation of the active length. The active length estimated using the initial elastic modulus of the soil may yield the active length less than the actual effective active length.

The effects of the mass oscillating with the pile are investigated in the present study. It is shown that considerably high bending moments are developed at the pile head due to the inertial effects. The developed bending moment in the pile clearly indicates that the interface bending moments are also increased with the mass on the pile head. Further, the increase in the pile top bending moment takes place at a higher rate than the interface bending moment. However, the variation of the pile top and interface bending moment with the mass at the pile head should be investigated further to quantify the effects of different parameters on



the variation of the bending moments. The results of the present study explain the reasons for failure of large number of flyover bridges during earthquakes as the effective mass on the pier head is considerably high for such structures.

Acknowledgement

This study was conducted during the author's fellowship research at Imperial College London, UK. The author wishes to acknowledge the support given by the Commonwealth Scholarship and Fellowship Commission, UK for making this study possible. Further, valuable suggestions from Prof. D. M. Potts, and Drs. S. Kontoe and L. Zdravkovic of the Department of Civil Engineering, Imperial College London are highly appreciated.

Reference

- i. Boulanger, R. W., Curras, C. J., Kutter, B. L., Wilson, D. W., and Abghari, A., 1999, Seismic soil-pile-structure interaction experiments and analyses, *J. Geotech. Geoenviron. Eng.*, 125(9), pp 750 – 759.
- ii. Darendeli, M. B., 2001, Development of a new family of normalized modulus reduction and material damping curves, Doctor of Philosophy, University of Texas at Austin.
- iii. Gazetas, G. and Dobry, R., 1984, Horizontal response of piles in layered soils, *Geotech. Earthquake eng. Div. ASCE*, 110, pp 20 – 40.
- iv. Gazetas G., and Mylonakis, G., 1998, Seismic soil-structure interaction: new evidence and emerging issues, *Geotechnical earthquake engineering and soil dynamics III*, ASCE, *Geotech. Special Publ. No. 11* (ed. by Dakoulas, P., Yegian, M., and Holtz, R. D.).
- v. Guerreirs, P. G. H. M, 2008, The dynamic soil behaviour – test interpretation and numerical modelling, M. Sc dissertation, Imperial College, London, UK.
- vi. Kontoe, S., 2006, Development of time integration schemes and advance boundary conditions for dynamic geotechnical analysis, Ph.D Thesis, Imperial College London, UK.
- vii. Kuhlemeyer, 1979, Static and dynamic laterally loaded floating piles, *J. Geotech. Earthquake eng. Div. ASCE*, 105, pp 289 - 304.
- viii. Mizuno, H., 1978, Pile damage during earthquake in Japan (1923 – 1983), *Dynamic response of pile foundations*, ASCE, *Geotech. Special Publ. No. 11*, (ed. By Nogami), pp 53 – 78.
- ix. Novak, M., *Pile under dynamic loads*, 1991, 2nd Int. Conf. Recent adv. Geotech. Earthquake eng. Soil dyn., St Louis, pp 250 – 273.
- x. Potts, D. M, and Zdravkovic, L., 2001, *Finite Element Analysis in Geotechnical Engineering*, Thomas Telford, London.
- xi. Thilakasiri, H. S., Potts, D. M., Kontoe, S., and Zdravkovic, L, 2009, “Earthquake Induced Kinematic Forces on Pile Foundations in Layered Medium”, *Engineer, J. of the Inst. of Engr. Sri Lanka*, 42, October.
- xii. Zienkiewicz O. C., Bicanic, N. & Shen, F. Q., 1988, Earthquake input definition and the transmitting boundary condition, *Conf. in Advances in Computational Nonlinear Mechanics*, Editor St. Doltnis, I, pp. 109 – 138.

Effects of Large Retarder Overdose on Concrete Strength Development

W.P.S. Dias, M.A.N. Dewapriya, E.A.C.K. Edirisooriya and C.G. Jayathunga

Abstract: Retarders are used to delay the setting time of concrete. Retarder overdosing is not an uncommon problem, but its effects are not well understood. In this study, laboratory tests were conducted to determine the effect of retarder overdosing on the setting time and strength of concrete, using both cubes, and cores from a large specimen. It was found that overdose levels of 3 times the normal dosage had little effect on setting and strength development. Also, concrete with even 6 times the normal dosage of retarder did eventually set and gain strength. Tests were also conducted to determine cement setting time under different temperature and surface drying (wind) conditions, in order to make inferences regarding strength development of concrete surfaces compared to interiors.

Keywords: Retarder overdose, setting time, strength development, surface vs. interior

1. Introduction and Objectives

A large number of retarding admixture products are available in the market. Some of their desirable effects are described by the manufacturers, but there is no information on some other effects, such as the effect of overdosing, with no allowable over dosage limit being specified. Such overdosing can occur in practice due to faults in a retarder dispenser at a batching plant. There is also not much research literature on large overdosing of retarder admixtures. In this paper we review some of the existing knowledge regarding the effects of retarder overdosing on concrete strength development and setting time, and present the results of testing designed to achieve the following research objectives.

- (i) To find the setting times, and strength development with age, and depth of thick concrete sections, for concretes cast with multiples of normal retarder dosage.
- (ii) To make inferences about the quality of the surface and interior of a thick concrete section by studying the effect of wind and temperature on cement setting time.

2. Review of Existing Knowledge

There are three types of retarding admixtures recognized by ASTM C494-1988 [1]. Type B simply retards the hydration of Portland cement. Type D not only retards the hydration but also acts to disperse the cement particles and thereby provides water reduction. Type G is a high range water reducing and set retarding admixture. The most commonly used chemical retarder is the Type D variety and is referred to as a water reducing and retarding admixture. The active ingredient, usually organic in nature, is absorbed on the surface of cement particles and also imparts like and repelling charges to the surfaces. The shielding of the cement particles reduces their reactions with water and causes retardation; the repelling charges disperse the cement particles and enable water reduction [2].

Dodson [2] has pointed out that the presence of set retarding admixtures causes an increase in 28 day strength over a reference where no retarder is added. He used different quantities

Eng (Prof) W.P.S. Dias, PhD(Lond), DIC, CEng, FIE(Sri Lanka), MIMStructE, Senior Professor of Civil Engineering, University of Moratuwa;
M.A.N. Dewapriya, BScEng(Hons);
E.A.C.K. Edirisooriya, BScEng(Hons); and
C.G. Jayathunga, BScEng(Hons)



of Type D retarding admixtures up to 0.18% (solids by weight of cement), and found that strength and final setting time increased by up to 35% and 300 min. respectively. It appears that the slower formation of the concrete hydration products - due to the presence of the set retarding admixture - is responsible for the higher later strengths. As a result of using set retarding admixtures (Type B or D), the normal hydration processes are slowed down so that the very early strengths (e.g. 1 day) are lower. At the same time, the slower rates of formation of the hydration products give them a greater opportunity to align or organize themselves in the cement matrix and produce higher later strengths [2].

Ramachandran [3] has shown that in the presence of retarders, the early strengths of cement mortar are lower than that of the reference specimen with no retarder. The 1 day compressive strength reduced from 11.8 MPa down to 1.2 MPa at an addition rate of 2% of a phosphoric acid retarder. The 28 day strength increased from 45 MPa to 65 MPa for a 1% dosage but was 60 MPa at a 2% dosage.

Two cases of large retarder overdosing in practice have been investigated by the first author. In the first one, setting was delayed by 3 days. The 5 day strength of cubes cast at the factory from the delivered concrete gave an average cube strength of 22.8 MPa for a grade 25 concrete. The estimated equivalent potential cube strengths of cores extracted at the ages of 16 and 29 days were 26 MPa and 28 MPa respectively [4].

Another grade 25 concrete in a transfer slab took 10 days to set due to a retarder overdose of around 4 times the normal dosage. Cores extracted after 53 days yielded an estimated equivalent potential cube strength of 32 MPa and no significant difference was found between the concrete that had set normally and with delay [5].

Setting times of Portland cement paste containing 3 types of retarders with different dosages have been found to increase with

increasing dosages; the gaps between initial and final setting times also increased [3].

3. Materials and Methods

3.1. Materials

A commonly used brand of Portland limestone cement was used for the tests. The coarse aggregate size was 20 mm. Grading of both coarse and fine aggregates conformed to the limits specified in BS 882:1992 [6]. Pozzolite 300R was used as the set retarding admixture. The trade literature indicates that it has been formulated to meet the requirements of ASTM C494-1988 [1] for Type B and D admixtures and is a very commonly used retarder. The range of recommended dosages is 2 to 3.5 ml/kg of cement.

A well established mix for grade 25 concrete was used for the research. The target mean cube strength was 35 MPa at 28 days. The proportions, which have accounted for the water reduction due to the presence of the retarder, are as follows: cement - 331 kg/m³, water - 195 kg/m³, fine aggregate - 768 kg/m³, coarse aggregate - 1106 kg/m³, Pozzolite 300R - 993 ml/m³ (i.e. 3 ml/kg of cement, and towards the upper end of the recommended dosage range).

3.2. Tests on concretes

Castings were done for four different retarder dosages, namely a normal dosage of 3 ml/kg cement (designated "ND"), and 3, 4.5 and 6 times the normal dosage, designated "3ND", "4.5ND" and "6ND" respectively. The total volume of the casting was 0.18 m³. The concrete was used to fill 150 mm cubes, setting time containers and a large specimen of dimensions 0.75 m x 0.36 m x 0.39 m, the last dimension being the depth. The test programme allowed for 2 specimens per condition for cores and 3 specimens per condition for cubes; in some cases the latter was also reduced to 2, when testing durations had to be extended. Replication was very good in all cases.

A slump test was done for each casting. The concrete setting time tests were carried out according to ASTM C403-1986 [7] for each dosage and were repeated in order to obtain a replicate of the results.

Both the cubes and the large specimens were cured to simulate site conditions. Curing under damp hessian was carried out for 7 days, with specimens being in their moulds. At 7 days the cubes were demoulded. Strength testing of cubes and extraction of 75 mm dia. cores from the large specimens were planned for ages of 7, 14 and 28 days, but longer durations too had to be resorted to at higher overdosing levels. In fact, it was possible to extract the first set of cores from the 4.5ND specimen only after 49 days and from 6ND specimen after 119 days. The vertically drilled cores were sliced in order to take three 85 mm height core samples from the top, middle and bottom of the large (390 mm deep) specimen. Care was taken to discard the top 40 mm and bottom 25 mm from the long cores. Rebound hammer testing was also carried out on the large specimen with a vertically downward hammer orientation just before cores were extracted; this is because rebound hammer testing is often used in practice to ascertain the extent to which the concrete has hardened, in situations of delayed setting.

3.3. Cement setting time tests

The cement setting time test was carried out according to BS 4550: Part 3: 1978 [8]. The water/cement ratio required to give a paste of standard consistence was 0.3. Control specimen moulds were kept at the room temperature of around 31°C and 85% RH. Other specimen moulds were kept in an oven at a temperature of 53°C and sealed by placing a circular rubber ring on the circumference of the mould with a heavy steel plate on top of it. The purpose of sealing was to prevent moisture escaping from the cement paste, thus simulating the sealed condition in the interior of a thick concrete element. Yet other specimens were kept at 31°C but under a wind speed of 2.5 m/s, generated by an electric fan. The above tests were done with and without retarder (at the normal

dosage) and repeated in order to obtain replicates of the results; replication was very good.

4. Results and Discussion

4.1. Slump variation

Table 1 indicates the variation of slump with retarder dosage. It should be noted that the standard mix design accounted for the water reducing property of the retarder. However, no additional water reduction was made at higher dosages of the retarder. Especially in this context, although higher slump was expected at higher dosages, Table 1 indicates that the reverse was true. More experimentation is probably called for, prior to making definite conclusions.

Table 1 – Variation of slump with retarder dosage

Dosage (x ND)	Slump (mm)
1.0	210
3.0	190
4.5	190
6.0	175

4.2. Concrete setting time

The initial and final setting time results are shown in Table 2, together with the variation from the mean. The setting times for all retarder overdosed mixes are significantly greater than for the concrete mixes with the normal dosage of retarder. In addition, there appears to be considerable variability between replicates at a dosage of 6ND.

Table 2 – Variation of concrete setting time with retarder dosage

Dosage (xnd)	Setting time (h)					
	Initial			Final		
	Trial 1	Trial 2	Variation	Trial 1	Trial 2	Variation
1.0	11.1	9.1	(+/- 10%)	12.2	-	
3.0	39.4	42.4	(+/- 4%)	42.7	52.3	(+/- 10%)
4.5	32.7	44.1	(+/- 15%)	60.8	54.5	(+/- 5%)
6.0	31.9	80.8	(+/- 43%)	55.1	-	



Concrete cube strength development with age for different retarder dosages is shown in Table 3. Cubes with a normal retarder dosage have recorded the highest compressive strength at 28 days. The strength development of the concrete with a retarder dosage of 3ND is also only a little below that of the concrete with a normal retarder dosage. However there is a significant delay in strength gain at retarder dosages of 4.5ND and 6ND. Such delays would not be acceptable in concrete practice. Nevertheless, even at these high dosages the concrete does in fact gain in strength. Both the 98 day strength of the concrete with a retarder dosage of 4.5ND and the 119 day strength of the concrete with a retarder dosage of 6ND were greater than the 28 day strength of the normally dosed concrete. The fact that concretes with retarder overdosing do ultimately gain their strengths is in agreement with the literature [2,3]. This should not however be a license to concrete producers to be slack in quality control.

Table 3 – Average cube strength at different ages and retarder dosages

Age (days)	Average cube strength (MPa) for dosages of			
	ND	3ND	4.5ND	6ND
7	29	22	2	2
14	34	27	2	2
28	35	32	7	2
49	-	-	25	-
98	-	-	39	-

4.4. Concrete core strength development

Table 4 shows strength development (in terms of equivalent in-situ cube strength) with depth and time for the concretes tested. In all cases, top cores have recorded the lowest strength and in almost all cases the bottom cores the highest. Even where the bottom core strengths are not the highest, they are only marginally lower than the middle core strengths. This variation in strength is well documented and is due to better compaction of the concrete bottom layers and to bleeding and greater air contents in the top layers.

Table 5 shows the ratios between the bottom core equivalent in-situ cube strengths and corresponding test cube strengths for all the concretes tested. This is depicted graphically in Figure 1 too.

Table 5 and Figure 1 clearly show that (bottom) cores have recorded lower strengths compared to cubes at higher retarder dosages, although there appears to be a maximum in the ratio at a dosage of 3ND. Once again there is a difference between the behaviour of concretes with retarder dosages of ND and 3ND the one hand, and those with dosages of 4.5ND and 6ND on the other.

Table 4 – Variation of core strength with age, dosage and depth

Table 5 – Ratios of bottom core equivalent in-situ

Age (days)	Equivalent in-situ cube strength (MPa)									
	7		14		28		49		98	
Dosage	ND	3ND	ND	3ND	ND	3ND	4.5ND	4.5ND	4.5ND	6ND
Top	20.3	19.5	22.8	23.7	24.2	27.7	16.9	20.7	17.8	17.8
Middle	25.1	20.3	23.5	25.9	25.1	28.1	17.1	24.7	17.4	17.4
Bottom	25.9	25.2	27.1	25.4	30.0	29.6	17.3	24.6	23.6	23.6

cube strength to test cube strength

Age	Bottom core equivalent in-situ
-----	--------------------------------

(days)	cube strength/Test cube strength			
	ND	3ND	4.5ND	6ND
7	0.89	1.15	-	-
14	0.79	0.94	-	-
28	0.86	0.93	-	-
49	-	-	0.69	-
98	-	-	0.63	-
119	-	-	-	0.64

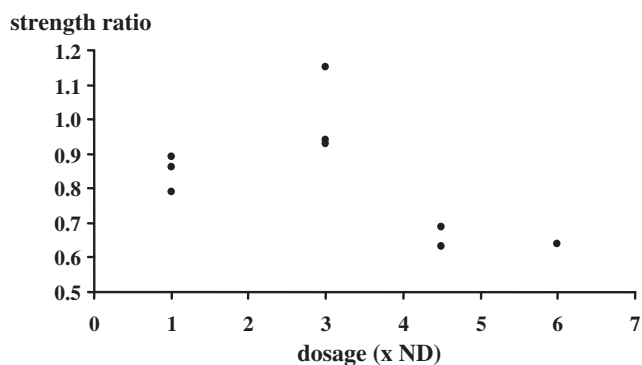


Figure 1 - Ratios of bottom core equivalent in-situ cube strength to test cube strength for different dosages

4.5. Rebound hammer tests on large specimens

The rebound hammer results were adjusted for the vertically downward orientation of the hammer and converted to estimated cube strength values, using a correlation that had been previously developed [9]. Table 6 shows the ratios between the strengths thus obtained and the equivalent cube strengths corresponding to the top cores for concretes with the two smaller retarder dosages at different ages.

The ratios for the normally dosed concrete are much higher than for the concrete with a retarder dosage of 3ND at all three ages. Also, all the ratios in the former case are greater than unity, and in the latter case less than unity. This suggests that the surfaces of overdosed concretes are weaker than the actual subsurface strength. Surfaces were so weak in concretes with larger retarder dosages that it was not possible to take rebound hammer readings up to 28 days for the 4.5ND case and even after 98 days for the 6ND one.

Table 6 – Ratios of “rebound strength” to top core strength

Age (days)	"Rebound strength"/Top core strength	
	ND	3ND
7	1.25	0.80
14	1.23	0.78
28	1.44	0.91

4.6. Cement setting time

The cement setting time results are indicated in Table 7 for specimens with and without the normal retarder dosage.

Table 7 – Cement setting time results

		With retarder	Without retarder
Control specimen (at 31 C ⁰)	Initial (h: min)	9:20	1:55
	Final (h: min)	12:40	2:45
Specimen at 53 C ⁰	Initial (h: min)	5:10	1:30
	Final (h: min)	7:30	1:55
Specimen at 2.5 m/s wind	Initial (h: min)	3:45	1:35
	Final (h: min)	5:05	2:10

Both increased temperature and increased wind speed cause reductions in setting time, but the reductions are greater in the specimens with the retarder. Table 8 indicates the corresponding percentage reductions, i.e. as percentages of the setting times for the control conditions (31°C and no wind). This table also shows that the reductions for the specimens with retarder are greater for the wind effect than for the temperature effect; the reverse is true for the specimens without the retarder. The effect of wind is ambiguous however, because stiffening will probably be due more to drying than to hydration.

Table 8 – Percentage reductions in cement setting time

	With	Without
--	------	---------



		retarder	retarder
At higher temperature	Initial	45%	22%
	Final	41%	30%
At higher wind speeds	Initial	60%	17%
	Final	60%	21%

4.7. Surface and interior quality

One aspects of importance in this study is the question as to whether the surface quality of retarder overdosed concrete is better or poorer than the interior, because it is surface tests (such as rebound hammer tests) that are mainly used in the field to monitor the hardening of concrete with delayed setting. The results from our study are somewhat ambiguous in this regard. On the one hand, as depicted in Table 6, the rebound number strengths are less than the top core strengths for concrete with a retarder overdose, thus indicating that the interior strength is better than that reflected by surface tests. On the other hand, equivalent cube strength results from cores are progressively lower than the corresponding cube test results, as retarder dosages increase, especially beyond 3ND (Table 5 and Figure 1). This suggests that strength development in large sections with retarder overdosing is slower than indicated by small specimens. The cement setting time tests also indicate that in retarded concretes the surface, if subject to wind, will stiffen (and perhaps harden) quicker than the interior, although the setting of the latter too will be accelerated by higher temperatures. This question of surface versus interior quality is clearly one that merits further investigation. Where thin sections are concerned differences between the surface and interior are likely to be less.

5. Conclusions

The following main conclusions can be drawn, based on this investigation that used the retarder Pozzolith 300R, an admixture made to satisfy the ASTM Type B and D requirements.

- 1) An overdose of retarder up to 3 times the normal dosage can be easily accommodated in concrete practice, with concrete strength gain not being appreciably affected.
- 2) Concrete with retarder overdoses of up to even 6 times the normal dosage will eventually reach or even exceed their corresponding 28 day strengths.
- 3) Equivalent cube strength results from cores are progressively lower than the corresponding cube test results, as retarder dosages increase.
- 4) Reductions in cement setting time for the specimens with a retarder are greater for the effect of a 2.5 m/s wind than for a temperature increase of 22°C above the ambient 31°C.
- 5) The question as to whether the interior quality of retarder overdosed concretes is better or poorer than the surface quality could not be resolved unambiguously, and requires further investigation.

References

- 1) ASTM C494. Standard specification for chemical admixtures for concrete. Philadelphia: American Society for Testing Materials, Vol. 04.02; 1988.
- 2) Dodson VH. Concrete Admixtures. New York: Van Nostrand Reinhold; 1990
- 3) Ramachandran VS, Feldman RF, Beaudoin JJ. Concrete science: Treatise on current research. London: Heyden; 1981.
- 4) Dias WPS. Delayed setting of concrete in foundations of Sahanaya mental rehabilitation centre. Technical Report, University of Moratuwa, 2004.



- 5) Dias WPS. Delayed setting of concrete transfer slab at 202 WA Silva Mawatha, Colombo 6. Technical Report, University of Moratuwa, May 2007.
- 6) BS 882: 1992. Specification for aggregate from natural resources for concrete. London: British Standards Institution; 1992.
- 7) ASTM C403. Time of setting of concrete mixtures by penetration resistance. Philadelphia: American Society for Testing Materials, Vol. 04.02; 1986.
- 8) BS 4550: Part 3: Section 3.6: 1978. Methods of testing cement: Test for setting time. London: British Standards Institution; 1978.
- 9) Dias WPS. Correlation of non-destructive test results with concrete strength. Engineer, Sri Lanka, March 1991, pp. 3-13.



Correlation among Hydraulic Parameters of Moving Hydraulic Jump in Rectangular Open Channels

M.C.M. Nasvi, Z.A.M. Asmeer, F.M. Mowsoom and K.P.P. Pathirana

Abstract: The moving hydraulic jump is a phenomenon, which is often observed in field conditions. Since the parameters of moving hydraulic jump vary with time, analytical equations cannot be used to derive relationships among hydraulic jump parameters. Experimental investigations were carried out to study the relationships among hydraulic parameters of a moving hydraulic jump in a rectangular flume. The flow parameters were recorded for the moving hydraulic jump produced for different sluice gate opening sizes. Based on the recorded data, flows parameters such as specific energy, flow rate and pressure force at downstream of the hydraulic jump were calculated. Also, using momentum and energy equations time independent relationships were obtained. The relationship among moving hydraulic jump parameters were obtained in non dimensional form. The correlations between stationary and moving hydraulic jump parameters such as specific energy, flow rate, pressure force and flow depth were derived.

Keywords: Specific Energy, hydraulic jump, bed friction, supercritical, sub critical

1. Introduction

Hydraulic jump is a phenomenon that occurs when the flow changes suddenly from supercritical to slow moving sub critical state. Experimental evidence suggests that flow changes from supercritical to sub critical state can occur very abruptly through a hydraulic jump. Sufficient theoretical aspects and equations are available for describing stationary state hydraulic jumps where jump parameters do not change with time. Often hydraulic jumps occur in field condition are not stationary. Due to various hydraulic structures such as control gates, weirs, sluice gates and culverts moving hydraulic jumps can be seen during their normal operation. The hydraulic parameters of the jump vary with the time. Also incident of moving jump occurs in events where obstructing structures are placed along the channel due to the unsteady flow conditions. These occurrences suggest the importance of the further studies to obtain sufficient knowledge on moving hydraulic jump. An analytical approach to study the hydraulic behaviour of the moving hydraulic jump has not been successful. Therefore any studies related to moving hydraulic jumps need to be studied based on laboratory experiments followed by data analysis. This paper presents a laboratory study conducted to investigate the correlation among hydraulic parameters of moving hydraulic jump in a rectangular flume. Even though most of the channels in the real practise are trapezoidal in shape, a rectangular

flume was used for the simplicity of analysis and considering the laboratory facilities.

2.0 Experimental Procedure

The flume having a rectangular cross section with width 0.3 m, depth 0.3 m and length 12 m was used for the experiment. A constant head tank was used to supply the water continuously through a recirculation path. The experimental setup is shown in Figure 1.

The study was conducted in two stages; the first stage of the experiment was dealt with the stationary hydraulic jumps and the second stage with moving hydraulic jumps. A sluice gate positioned at the head of the channel and a tail gate were used to generate hydraulic jumps in the channel. A rectangular grid was fixed on the glass side wall of the channel in order to measure the distances along the channel and corresponding water levels during the experiments.

M.C.M. Nasvi, B.Sc. Eng. (Hons.)(Peradeniya), Department of Civil Engineering, University of Peradeniya, Sri Lanka.
Z.A.M. Asmeer, B.Sc. Eng. (Hons.)(Peradeniya), Department of Civil Engineering, University of Peradeniya, Sri Lanka.
M.F. Mowsoom. B.Sc. Eng. (Hons.)(Peradeniya), Department of Civil Engineering, University of Peradeniya, Sri Lanka.
Eng.(Prof.) K.P.P. Pathirana, B.Sc. Eng. (Hons.)(Peradeniya), M.Eng., Ph.D(KULeuven), C.Eng., FIE(Sri Lanka), MICE(London), Professor of Civil Engineering, Department of Civil Engineering, University of Peradeniya, Sri Lanka.

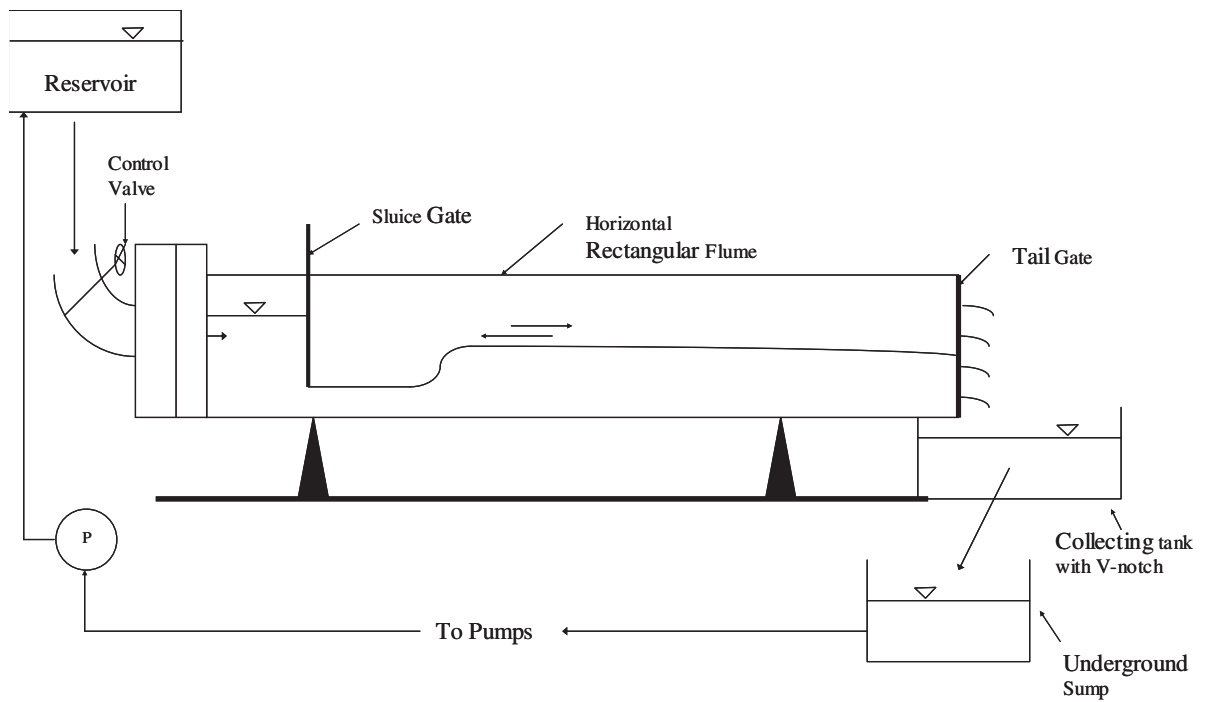


Figure 1: Experimental set-up

During the first stage of the study stationary hydraulic jumps were generated in the flume by adjusting the opening sizes of the sluice gate to 30 mm, 40 mm and 50 mm while keeping the same tail gate level. For each gate opening size, the water depth upstream of the sluice gate was increased in 10 mm steps by increasing the flow rate in the channel from 8 l/s to 26 l/s using the control valve. Once the steady state analysis was completed, the moving hydraulic jump was formed for the same flow range by changing the control valve gradually. This moving jump was recorded by two video cameras. Then the required data such as, water level upstream of the sluice gate and super critical and sub critical depths, position of the jump, length of the jump and the time taken to reach the corresponding upstream depth were recorded by digitizing the recorded video.

3.0 Results

3.1 Stationary Hydraulic Jump

The flow parameters such as discharge (Q), supercritical depth (Y_{1s}), subcritical depth (Y_{2s}), position of the jump toe (X_{js}) from the sluice gate, supercritical and subcritical flow velocities

were recorded for each 10 mm increment in upstream water depth (Y_3). The schematic diagram of the sluice gate is shown in Figure 2. The momentum equation is applied to stationary jump to derive a functional relationship for bed friction (F):

$$\frac{1}{2} \gamma Y_{1s}^2 - \frac{1}{2} \gamma Y_{2s}^2 - F = \rho q (V_{2s} - V_{1s}) \dots \dots (1)$$

Using the continuity equation;

$$q = V_1 Y_1 = V_2 Y_2; V_2 = \frac{V_1 Y_1}{Y_2} \dots \dots \dots (2)$$

Combining Eqns.(1) and (2),

$$F = \frac{\rho g (Y_{1s}^2 - Y_{2s}^2)}{2} - \frac{\rho q}{b} (V_{2s} - V_{1s}) \dots \dots \dots (3)$$

where, subscript 1 denotes supercritical section and 2 denotes subcritical section, subscript s denotes stationary hydraulic jump condition, Y- Flow depth, V- velocity of the flow, ρ -density of water, Q- flow rate and F_r - Froude number. The variation of bed friction (F) with flow rate (Q) and flow rate (Q) Vs position of the jump toe (X_{js}) are shown in Figures 3 and 4, respectively.



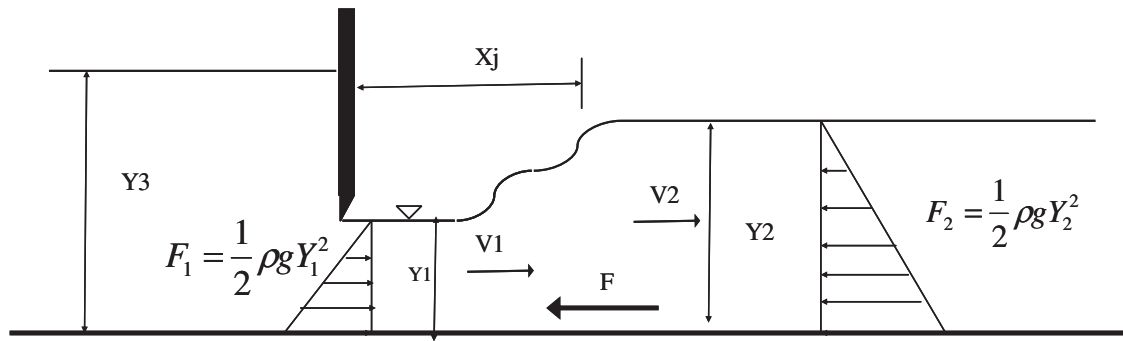


Figure 2: The schematic diagram of sluice gate and hydraulic jump

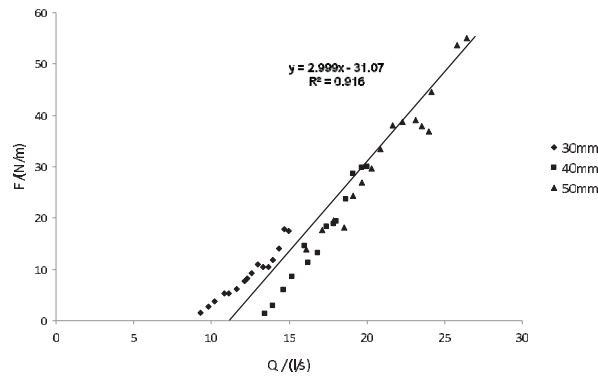


Figure 3: The variation of bed friction (F) with flow rate (Q)

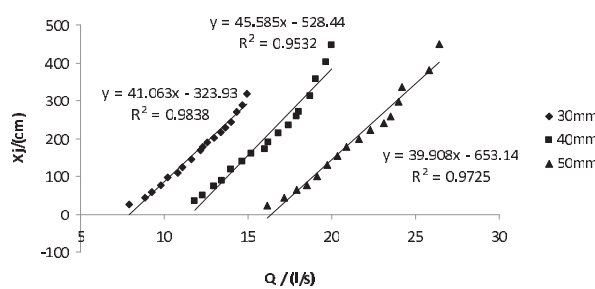


Figure 4: Position of the hydraulic jump (Xj) Vs Flow rate (Q)

3.2 Moving Hydraulic Jump

Three different hydrographs were plotted for each opening size (30 mm, 40 mm and 50 mm) at the upstream sluice gate. Figure 5 shows the recorded flow hydrographs.

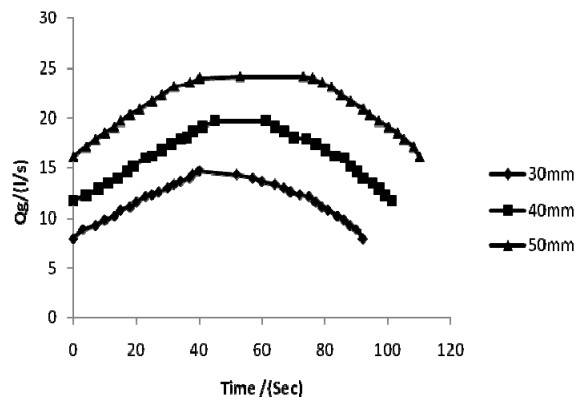


Figure 5: Recorded flow hydrographs for different gate openings

In order to present the results, moving hydraulic jump variables are listed as follows; supercritical depth (Y_{1u}), subcritical depth (Y_{2u}), specific energy at the downstream section (E_{2u}), flow rate at the gate (Q_g), flow rate at the downstream section (Q_{2u}), pressure force at the downstream section (F_{p2u}) and density of water (ρ). The subscripts 1 and 2 indicate the variables associated with supercritical flow upstream and subcritical flow downstream of the moving jump while, subscripts s and u denotes the stationary and unsteady flow conditions, respectively. The relationship between E_{2u} and E_{2s} can be obtained using the energy equation as follows;

$$E_{2s} - E_{2u} = Y_{2s} - Y_{2u} + \frac{1}{2g}(V_{2s}^2 - V_{2u}^2) \dots \dots (4)$$

Then the task is to find out an empirical formula to estimate the flow rate at the downstream section (Q_{2u}). For this purpose a graph is plotted for specific energy difference ($E_{2u} - E_{2s}$) against depth difference ($Y_{2u} - Y_{2s}$) as shown in Figure 6.

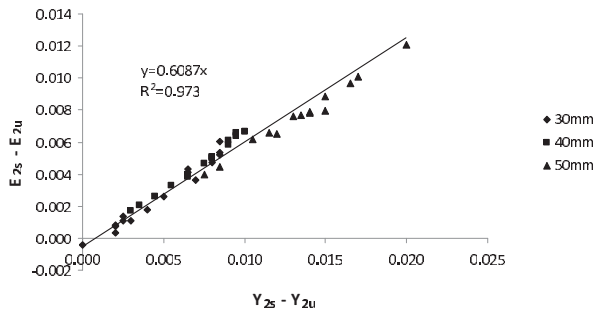


Figure 6: The variation between specific energy difference ($E_{2s} - E_{2u}$) and depth difference ($Y_{2s} - Y_{2u}$)

From the above graph the following relationship was obtained;

$$E_{2s} - E_{2u} = 0.608(Y_{2s} - Y_{2u}) \dots \dots \dots (5)$$

Then, substituting the terms for Eq. (3.5) from Eq. (3.4) gives;

$$Y_{2s} - Y_{2u} + \frac{1}{2g}(V_{2s}^2 - V_{2u}^2) = 0.608(Y_{2s} - Y_{2u})$$

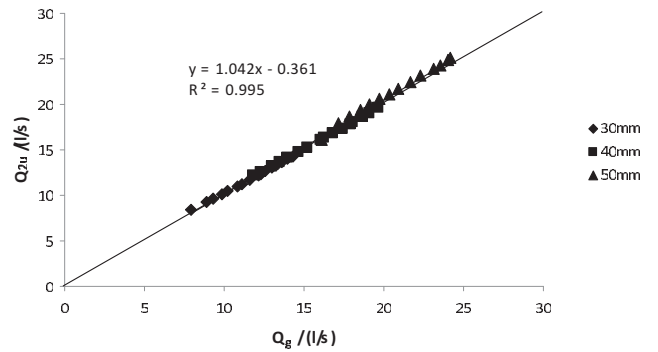
$$Q_{2u} = \sqrt{\frac{Q_g^2}{Y_{2s}^2} - 7.691b^2(Y_{2s} - Y_{2u})} \dots \dots \dots (6)$$

Using the above equation Q_{2u} values for different opening sizes were calculated. Once Q_{2u} was obtained the relationship between moving hydraulic jump parameters were obtained. The variations are shown in Figure 7.

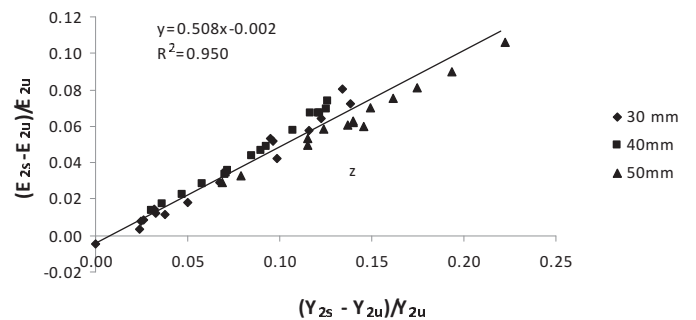
Then applying the momentum equations for the control volume;

$$F_{p1u} - F_{p2u} - F = \frac{\rho}{b^2} \left(\frac{Q_{2u}^2}{Y_{2u}} - \frac{Q_g^2}{Y_{1u}} \right) \dots \dots \dots (7)$$

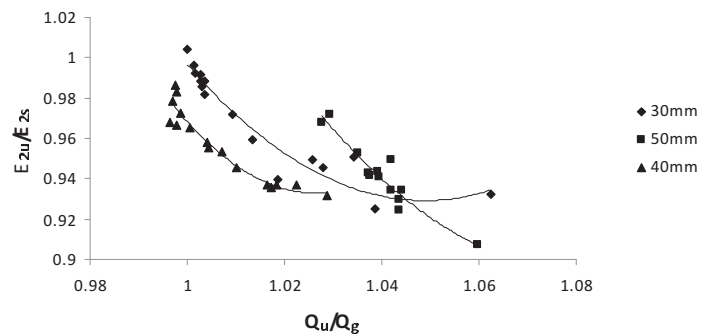
$$F_{p2u} = \frac{\rho g Y_{1u}^2}{2} - F - \frac{\rho}{b^2} \left(\frac{Q_{2u}^2}{V_{2u}} - \frac{Q_g^2}{Y_{1u}} \right) \dots \dots \dots (8)$$



(a)



(b)



(c)



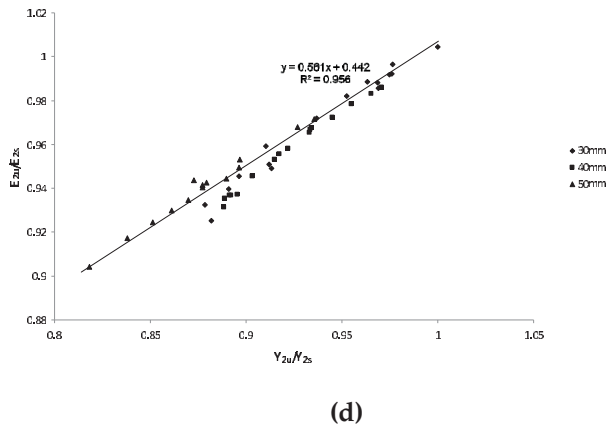


Figure 7: (a) Flow rate at the downstream section (Q_{2u}) against Flow rate at gate (Q_g) (b) relative specific energy difference $\{(E_{2s} - E_{2u}) / E_{2u}\}$ against relative depth difference $\{(Y_{2s} - Y_{2u}) / Y_{2u}\}$ (c) Specific energy ratio (E_{2u} / E_{2s}) against flow rate ratio (Q_u / Q_g) (d) specific energy ratio (E_{2u} / E_{2s}) against depth ratio (Y_{2u} / Y_{2s}).

Then F_{p2u} was plotted against Q_g for each opening size, as shown in Figure 8.

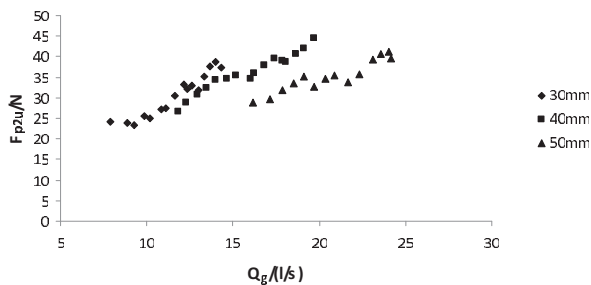


Figure 8: The variation between pressure forces at the downstream (F_{p2u}) and Flow rate at gate (Q_g)

4.0 Discussion

Bed Friction (F) linearly varies with the flow rate (Q). Flow rate at downstream section (Q_{2u}) has a linear variation with the flow rate at gate (Q_g). Q_{2u} is approximately equal to Q_g for smaller flow rates whereas it varies linearly for higher flow rates (see Figure 7 (a)).

Q_{2u} is the most dominant factor which affects all the other jump parameters of a moving hydraulic jump. Relative specific energy difference $\{(E_{2s} - E_{2u}) / E_{2u}\}$ is proportional to

relative depth difference $\{(Y_{2s} - Y_{2u}) / Y_{2u}\}$ for all the flow rates (see Figure 7 (b)). Since the downstream flow rate for moving jump is different from that of the stationary jump for the same upstream flow depth there is a specific energy difference. That difference is related to the difference in subcritical water depths. Specific energy ratio (E_{2u} / E_{2s}) decreases with flow rate ratio (Q_u / Q_g) for each opening sizes (see Figure 7 (c)).

Pressure force at the downstream section (F_{p2u}) increases with flow rate (Q_{2u}) for all the flow rates. Specific energy ratio (E_{2u} / E_{2s}) has a linear variation with depth ratio (Y_{2u} / Y_{2s}) for all the flow rates (see Figure 7 (d)). This result can easily be interpreted if the derivation of Energy Equation is considered, because specific energy of a moving hydraulic jump is depending on Y_{2u} and V_{2u} . There is a small difference between the values of Y_{2u} and Y_{2s} , V_{2u} and V_{2s} . This small variation may cause the linear variation.

The formula derived for flow rate (Q_{2u}) in the downstream of moving hydraulic jump is;

$$Q_{2u} = \sqrt{\frac{Q_g^2}{Y_{2s}^2} - 7.691b^2(Y_{2s} - Y_{2u})} \dots \dots \dots (9)$$

The following formula was obtained for downstream pressure force of moving hydraulic jump;

$$F_{p2u} = \frac{\rho g Y_{1u}^2}{2} - F - \frac{\rho}{b^2} \left(\frac{Q_{2u}^2}{V_{2u}} - \frac{Q_g^2}{Y_{1u}} \right) \dots \dots (10)$$

5.0 Conclusions and Recommendation

A series of experiments were conducted in a laboratory open channel to derive the relationship among moving hydraulic jump parameters. The correlation between stationary and moving hydraulic jump parameters were obtained in a non-dimensional form incorporating the bed friction of the flume.

There were some linear relationships between jump parameters which was independent of the gate opening size. Some of the relationships were non-linear and those were depending on

the gate opening size. Bed friction varies linearly with the flow rate. There is a difference in pressure across the jump front which changes from hydrostatic value at the gate to a value higher than that at the downstream. It was observed that pressure force at downstream depends on flow rate at the gate, downstream flow rate, bed friction, super critical depth and subcritical depth for a moving hydraulic jump. An empirical formula for the flow rate at downstream for moving hydraulic jump was obtained using theoretical expressions and experimental results.

It was also observed that the flow rate at the downstream section is equal to the flow rate at the gate for smaller discharges whereas downstream flow rate is higher than the flow rate at the gate for higher flow rates. Also it was found that Specific Energy for stationary jump (E_{2s}) was greater than the energy for moving jump (E_{2u}) and this reduction is due to higher losses in moving hydraulic jump. This higher loss indicates the presence of turbulence.

Laboratory experiments covering a wide range of discharges are recommended to verify the results obtained during this study. Since most of the open channels in the field applications are trapezoidal in shape, this study could be extended for open channels having trapezoidal cross sections to investigate the dynamic behaviour of hydraulic jumps in these channels that could be very useful in field applications. In addition, the experiments with different boundary roughness and channel slopes are also needed for a complete study.

References

1. Araz M. Charangic and M. Hanif Chaudhry, "Numerical Simulation of Hydraulic Jump", ASCE, Journal of Hydraulic Eng., Vol-117, pp (1195-1211), 1991.
2. Hubert Chanson, "Dynamic Similarity and Scale Effects Affecting Air Bubble Entrainment in Hydraulic Jumps", 6th International Conference on Multiphase Flow, Germany, July, ICMF, pp (1-11), 2007.
3. Iwao Ohtsu, Youichi Yasuda, "Hydraulic Jump in Sloping Channels", ASCE, Journal of hydraulic Eng., Vol-117, pp (905-921), 1991.
4. Joel W. Toso, and C. Edward Bowers, ASCE, "Extreme Pressure in Hydraulic Jump-Stilling Basins", ASCE, Vol 114, pp (829-843), 1988.
5. Jung-fu yen, Chih-Han Llin and Chang-Tai Tsai, "Hydraulic Characteristics and Discharge Control of Sluice Gates" Journal of the Chinese Institute of Engineers, Vol -24, no 3, pp (301-310), 2001.
6. Kim.W. and K.Y. Han. "Computation of Transcritical Flow by Implicit ENO Scheme", 4th International Conference on Hydro-science and Engineering, September, pp (26-29), 2000.
7. Montes J.S. and H. Chanson, "Characteristics of Undular Hydraulic Jump Experiments and Analysis", ASCE, Journal of Hydraulic Eng, Vol-124, pp (192-205), 1998.
8. Nalluri.C. & R.E. Featherstone, Balckwell Publishing, Fourth Edition, "Civil Engineering Hydraulics", pp (204-209), 2001
9. Richard H. French, Mcgraw-Hill, International Edition, "Open Channel Hydraulics", pp (79-102), 1986.
10. Rizi Parvaresh A., S. Kouchakzadeh and M.H. Omid, "A Study of Moving Hydraulic Jump in Rectangular Channels", Journal of Applied Science 6 (5), pp (1192-1198), 2006.
11. Tseng, M.H., C.A. Hsu and C.R Chu, "Channel Routing in Open-Channel Flow with Surges", ASCE, Journal of Hydraulic Eng., Vol-127, pp (115-122), 2001.



Forecasting Thermal Stratification of the Victoria Reservoir using a Hydrodynamic Model

K.D.W. Nandalal, S. Piyasiri and K.G.A.M.C.S. Abeysinghe

Abstract: Strong thermal stratification in a reservoir may result in oxygen depletion along the vertical profile downwards leading to its eutrophication. The paper is an investigation of thermal stratification behaviour of the Victoria reservoir in Sri Lanka, which experienced several water quality linked problems in the past. A one-dimensional reservoir hydrodynamics model is calibrated and validated for the Victoria reservoir. The calibration and validation are strengthened by calculating several goodness-of-fit statistics. The study further shows the possibility to change the strong thermal stratification of the Victoria reservoir by manipulating the releases from it. The model that ensures a reasonable prediction of thermal stratification enables taking precautionary measures to avoid adverse reservoir water quality conditions.

Keywords: Reservoir, Thermal stratification, Hydrodynamic modeling

1. Introduction

When a flowing river is dammed and becomes an impoundment two major changes, which have a marked effect on water quality, occur. Firstly, creating an impoundment greatly increases the time required for water to travel the distance from the headwaters to the discharge at the dam. Secondly, thermal or density and therefore, chemical stratification may take place. Both increased detention time and thermal stratification frequently cause adverse water quality conditions in reservoirs.

The desire to manage the quality of water stored in reservoirs led to the development of numerical models for the simulation of internal dynamics of them. Lakes or reservoirs that do not show significant thermal stratification during the yearly cycle could be modeled assuming complete mixing is occurring throughout its volume during the whole year (O'Connor & Mueller 1970; Nandalal 1995). However, for reservoirs in which the foregoing condition does not apply, complex models have to be developed to predict thermal gradients, density stratification and the impact that various operating rules may have on these and other physical, chemical and biological quality characteristics of the impoundment water.

Much of the development in modeling reservoir dynamics has been done by assuming one-dimensionality, where vertical motion is inhibited and transverse and longitudinal variations are quickly evened out. Even with this simplification, it is difficult to model the

interactions of a number of complex processes occurring in a reservoir. Over the last several decades diverse models of varying complexity and success have been produced (Dake & Harleman 1969; Huber *et al.* 1972; Markofsky & Harleman 1973; Imberger *et al.* 1978; Imberger & Patterson 1981; Hostetler & Bartlein, 1990).

There has also been to a less extent some development of two and three dimensional stratification models. However, the increasing complexity and computational requirements have severely limited their development. Although three dimensional models describe the water quality and ecology of reservoirs better, one dimensional models remain attractive, appropriate and convincing for understanding the physical processes occurring in reservoirs (Orlob 1983; Hamilton & Schladow 1997; Joehnk & Umlauf 2001, Abeysinghe *et al.* 2005).

Dynamic Reservoir Simulation Model (DYRESM) is a one-dimensional numerical model that can simulate thermal behaviour and water quality distribution in a reservoir and predict the distribution of temperature (and therefore, density) in reservoirs in response to

Eng (Prof) K.D.W. Nandalal, C Eng., FIE(SL), BScEng, MEng, PhD, Professor of Civil Engineering, Department of Civil Engineering, University of Peradeniya.

Prof. S. Piyasiri, BSc, PhD, Senior Professor of Zoology, Department of Zoology, University of Sri Jayawardenapura.

K.G.A.M.C.S. Abeysinghe, BSc, MPhil

meteorological forcing, inflow and outflow. The model provides a means of predicting seasonal and inter-annual variability of lakes and reservoirs as well as sensitivity testing to long-term changes in environmental factors or watershed properties.

Several reservoirs in the Mahaweli Project experienced water quality linked problems in recent times. The model DYRESM was calibrated and validated for the Victoria reservoir to predict water level, temperature, salinity and density in it. Calibration and validation were strengthened by calculating several goodness-of-fit statistics.

The paper first presents a brief description of the Victoria reservoir and its catchment. It is followed by descriptions of DYRESM and the statistical methods used in the study. Analysis carried out including calibration and verification of the model for the Victoria reservoir, a statistical analysis, a study on the impact of releases on reservoir thermal

stratification are provided next. Finally the conclusions are given.

2. Site Description

Victoria reservoir (Figure 1) is a large deep water body resulted from the “Mahaweli Development Scheme” due to construction of a dam across the river Mahaweli in Sri Lanka in 1983, mainly for hydroelectric power generation. Table 1 presents general and morphometric characteristics and physico-chemical data of the Victoria reservoir. The Victoria reservoir receives water from its catchment of approximately 1891 km². It gets water from Hulu River and Mahaweli River (releases from Kotmale reservoir via Polgolla barrage).

Table 2 presents monthly averages of climatological data collected at a recording station close to Victoria dam over the period from 1992 to 1999.

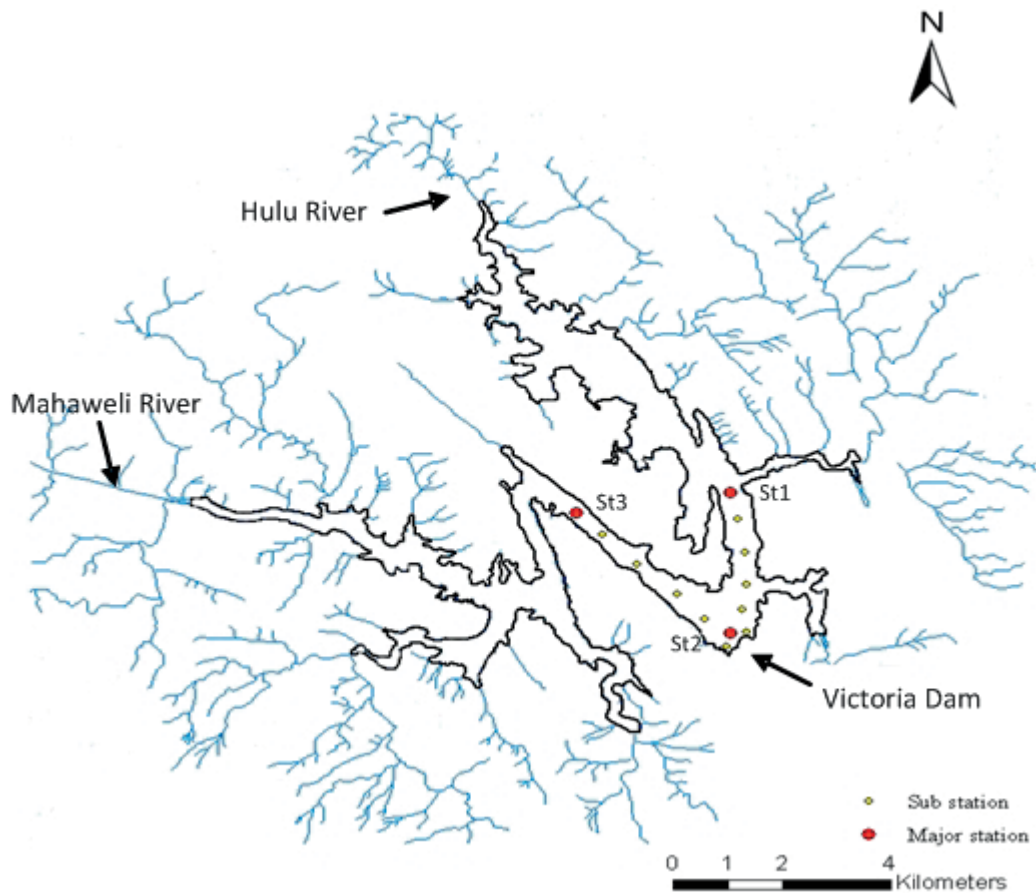


Figure 1 - Sampling stations and major inflowing rivers of the Victoria reservoir

Table 1 - General and morphometric characteristics and Physico-chemical data of the Victoria reservoir

(a) General Characteristics	
Latitude	7° 15' N to 7° 19' N
Longitude	80° 39' E to 80° 48' E
Full supply level	438.0 m MSL
Extreme flood level	441.2 m MSL
Minimum operating level	370.0 m MSL
Storage capacity (at Full supply level)	721.2×10 ⁶ m ³
(at Minimum operating level)	34.0×10 ⁶ m ³
Catchment area	1891 km ²
Major inflowing rivers	Mahaweli River, Hulu River
Minor inflowing rivers	Galmal Oya, Mool Oya, Thalathu Oya, Kiwiliyadda Oya, Kapuliyadda Oya,
Outflowing river	Mahaweli river
(b) Morphometric Characteristics	
Surface area	21.14 km ²
Maximum length	6.8 km
Maximum breadth	2.41 km
Maximum depth	98 m
Mean depth	30.5 m
Shore line (SL)	165 km
Mean river flow	105 m ³ /sec
(c) Physio-chemical data	
Surface temperature	24.8 – 31.2 °C
Hypolimnion temperature	24.2 °C
Conductivity (surface)	53.3 – 105.2 µS cm ⁻¹
pH (surface)	6.03 – 8.65
Transparency (Secchi disk)	0.65 – 3.25 m
Temperature (inflowing rivers)	22.4 – 27.2 °C

Table 2 - Average monthly climatological elements of the Victoria reservoir for the period 1992-1999

	Jan	Feb	Mar	Apr	May	Jun	Jul	Aug	Sep	Oct	Nov	Dec	Total
Rainfall (mm)	194	95	46	93	65	40	36	72	76	188	193	162	1259
Temperature													
Average (°C)	23.6	24.8	26.0	27.4	28.0	26.8	27.0	26.2	26.8	25.8	25.0	23.6	
Maximum (°C)	27.6	29.2	31.8	32.6	33.0	31.4	31.2	31.2	30.8	30.0	29.4	28.0	
Minimum (°C)	19.8	20.2	20.2	22.0	22.8	22.6	22.8	22.0	22.8	21.4	20.8	19.6	
Wind speed (km/h)	2.8	2.0	1.7	2.4	3.6	5.6	5.8	5.2	3.2	2.7	2.1	2.0	
Evaporation (mm)	78	76	121	88	114	104	106	96	104	71	62	57	1077
Sunshine hours	6.8	6.8	8.9	6.6	7.8	4.8	4.8	5.5	6.5	5.7	6.1	6.1	

The table describes that the lowest temperatures occur from January to February and November to December and the highest

temperatures occur from April to September. Rainfall varies considerably during the year. Highest rainfall occurs in January and from

October to December. Wind speed varies considerably (measured at 2 m above ground surface) during the year. The mean monthly wind speed is highest in June to August and lowest in the period from January to April and from October to December. The average annual evaporation around the Victoria reservoir is 1077 mm. Monthly variation of evaporation follows the mean temperature and total radiation variations.

Limnological investigations have been conducted (Piyasiri 1991) since 1987 to understand the trophic nature of the reservoir. Piyasiri (1991) concluded that the Victoria reservoir is a tropical oligomictic water body. The Victoria reservoir faced several water quality related problems in the past. It reached a pre blooming stage in March 2003 indicating high densities of *Microcystis aeruginosa* when reservoir was filled up to two third of its full capacity. This indicates its high sensitivity towards eutrophication and blooming.

3. Methodology

3.1 Hydrodynamic Model: DYRESM

The assumption of one-dimensionality in DYRESM is based on the density stratification usually found in lakes and reservoirs, which inhibits vertical motions while lateral and longitudinal variation in density are quickly relaxed by horizontal convection, occurring on time scales shorter than vertical advection. The model has been developed with emphasis on parameterization of the physical processes rather than numerical solution of the appropriate differential equations.

DYRESM uses a Lagrangian layer scheme in which the reservoir is represented by a series of horizontal layers of uniform property but of variable thickness. As inflows and outflows enter or leave the reservoir, the affected layers expand or contract and those above move up or down to accommodate the volume change. The vertical movement of layers is accompanied by a thickness change as the layer surface areas change with vertical position in accordance with the reservoir bathymetry. Mixing is modeled by amalgamation of adjacent layers, and the layer thicknesses are dynamically set internally by the model to ensure that for each process, an adequate resolution is obtained.

Even with the assumption of one-dimensionality, the vertical density structure is the result of a complex interaction of a number of processes active in lakes and reservoirs. These individual processes are parameterized in DYRESM. The development of DYRESM is described in detail in the literature (Imberger *et al.* 1978; Imberger and Patterson 1981, Patterson *et al.* 1984), including descriptions of the process parameterizations. The processes included in the model are surface heat, mass and momentum exchanges, surface mixed layer deepening model, inflow, outflow, mixing in the hypolimnion and bubble plume destratification.

The model is constructed as a main programme with subroutines, which separately model each of physical processes of inflow, withdrawal, mixed layer dynamics and vertical transport in the hypolimnion. In addition there are a number of service subroutines, which provide maintenance of the layer system (volume, position, etc.) and provide calculations of physical properties, which are frequently required such as density. The functions of the main programme are therefore of input/output, the calculation of fixed parameters and control over timing of the calls to the various process subroutines.

The data required for the DYRESM model are daily values of air temperature, relative humidity, wind velocity, solar radiation, rainfall, evaporation, inflow quantity, inflow quality and outflow quantity.

The model DYRESM has been used widely to study behaviour of reservoirs (Imberger 1981, Spigel and Ogilvie 1985, Campos *et al.* 2001, Antenucci *et al.* 2002, Gal *et al.* 2003, Nandalal *et al.* 2005).

3.2 Statistical Analysis (Fit statistics)

The ability of the model to simulate observed conditions was tested with two goodness-of-fit statistics: the root mean squared error (RMSE), and the mean of the relative absolute error (MRAE).

The RMSE is defined as the square root of the mean of the squared difference between observed and simulated values.

$$RMSE = \sqrt{\frac{1}{n} \sum_{i=1}^n (x_{s,i} - x_{o,i})^2} \quad (1)$$



Where, $x_{s,i}$ and $x_{o,i}$ are the simulated and observed i^{th} values and, n is the sample size. In this analysis, the root mean square error was used as the measure of error between computed and observed temperatures.

As such, the RMSE is similar to a standard deviation of the error (Rounds and Wood, 2001), roughly two-thirds of the errors are expected to fall within ± 1 . RMSE values have the units of the quantity of interest, and lower values indicate a better fit. For the statistic to be relevant, however, one must know the range of the fitted data to determine whether an RMSE indicates an excellent or poor fit.

The MRAE is the mean of the absolute value of relative errors. Lam *et al.* (1983) expressed this statistic as the following,

$$MRAE = \frac{1}{n} \sum_{i=1}^n \frac{|x_{o,i} - x_{s,i}|}{x_{o,i}} \quad (2)$$

Variables are as defined before.

There are limitations for using the above equation, specifically, there is poor behaviour of MRAE at low values of $x_{o,i}$ and the variability of the data is not adequately recognized. The MRAE is also constrained if $x_{o,i}$ is much greater than $x_{s,i}$. However, an advantage of the MRAE is that this statistic is a readily understood comparison and can provide a gross measure of model adequacy and can be useful in comparing models.

3.3 Data collection

The study area of the reservoir and its tributaries are depicted in Figure 1. Water samples have been collected once a month from three stations St.1, St.2, and St.3, vertically from top to bottom at 10 m intervals. Physical, chemical and biological water quality parameters measured in these water samples are temperature, dissolved oxygen concentration, electrical conductivity, pH, chloride, total alkalinity, suspended solids, nitrogen, ammonia, nitrate, nitrite, biological oxygen demand, fluoride, heavy metals, chlorophyll and phytoplankton. This study uses the data collected at the station St.2. These water quality data have been collected through limnology project at Mahaweli reservoirs by the Department of Zoology, University of Sri Jayawardenapura, Sri Lanka (Piyasiri, 1996).

The daily values of air temperature, relative humidity, wind velocity, rainfall, evaporation, reservoir inflow quantity, inflow quality and outflow quantity, which are required for the model were collected from Headworks Administration, Operation and Maintenance unit of the Mahaweli Authority of Sri Lanka. Actual duration of sun shine hours, which were used to estimate solar radiation, were collected from Natural Resource Management Centre at Peradeniya, Sri Lanka.

4. Analysis

4.1 Data for the model

The DYRESM model for the Victoria reservoir was calibrated using the data collected during 1995. Except short wave radiation and daily inflow temperatures, all the other data required for the model were available for that year. However, records of daily sunshine duration were available for the area. Using that, the short wave radiation were estimated based on the Angstrom formula (Allen *et al.* 1998), which relates solar radiation to extraterrestrial radiation and relative sunshine duration.

Maximum possible duration of sunshine hours and extraterrestrial radiation for different latitudes listed in FAO publication No.56 were adopted in the study (Allen *et al.*, 1998). The constants in the Angstrom formula were obtained from the modified Fre're curves for Sri Lanka by Samuel (2000). Daily inflow temperatures were estimated as the average of the air temperatures during the 4 days preceding the date of the inflow entering the reservoir, as suggested by the model developers.

Initial reservoir water level, temperature and salinity are required to start a simulation. Initial water level was set to the observed water level of the reservoir on the first day of simulation period. Observed water temperature and salinity profiles at St.2 on that day were available for the initial condition of the reservoir.

4.2 Model parameters

The model parameters are given in Table 3. However, many of them cannot be measured directly and were obtained by a trial and error procedure of comparing the temperature

obtained from the model DYRESM simulations with observations. Most of the hydrodynamic and thermal processes in a reservoir are simulated in the DYRESM model. The mean albedo of water, emissivity of water surface and light extinction coefficient were found to be very sensitive parameters, while the other parameters were relatively insensitive.

A large number of simulations with DYRESM were carried out by changing model parameters until the simulated temperatures were very close to the observed data, for the period 9th January to 31st December 1995 for the

Victoria reservoir. The adopted model calibration process is described below.

4.3 Reservoir mass balance

The model gives reservoir water level during the simulation period. It was compared with the observed reservoir water levels during the simulation period from 9th January to 31st December 1995, and they were found to be in good agreement as shown in Figure 2. RMSE between measured and simulated water levels was 0.03 m. The difference between measured and simulated water levels ranged from -0.17 to 0.32 m, and the mean difference was 0.06 m.

Table 3 - Parameters of the DYRESM model for the Victoria reservoir

Parameter	Value
Neutral 10 m aerodynamic drag coefficient	1.3×10^{-3}
Mean albedo of water	0.5
Emissivity of a water surface	0.99
Light extinction coefficient	0.4
Critical wind speed at 10 m height [m s ⁻¹]	4.00
Time of day for output (in seconds from midnight)	43200
Entrainment coefficient constant	2.0×10^{-3}
Bubbler entrainment coefficient	0.006
Buoyant plume entrainment coefficient	0.083
Shear production efficiency	0.06
Potential energy mixing efficiency	0.20
Wind stirring efficiency	0.06
Effective surface area coefficient	1.0E+07
Vertical mixing coefficient	200

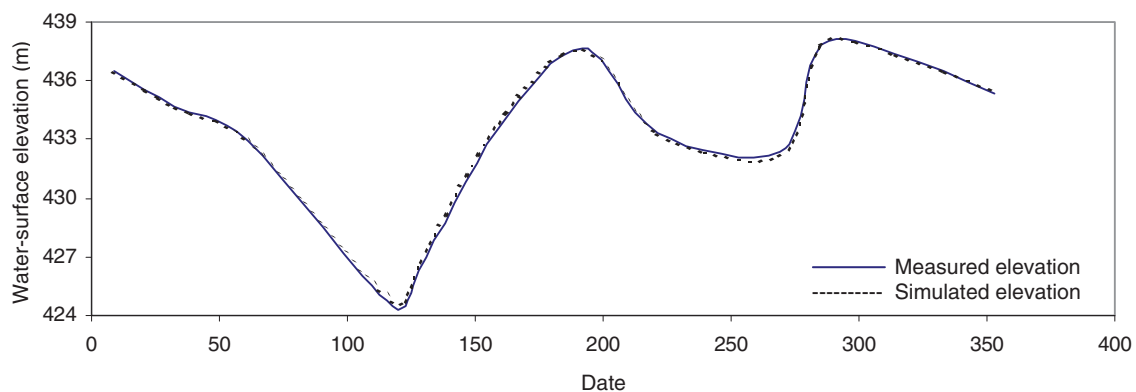


Figure 2 - Observed and simulated reservoir level in the Victoria reservoir at St 2 during calibration

4.4 Temperature variation

The effects of inflow water temperature, surface heat exchange (which includes the effects of solar radiation and wind), bottom heat exchange, transport of heat, and internal mixing (including the effects of the withdrawal at the

Victoria dam) are included in the simulation of water temperature.

The DYRESM simulated water temperatures (118 observations) from January through December 1995 were compared with corresponding observed values for St 2 during



the calibration stage to decide the model parameter values. In Figure 3 the simulated and measured vertical reservoir water temperature profiles at different days of the year are presented. The model simulates the onset of stratification, mixed layer depth and water temperatures quite accurately. Measured water temperatures ranged from 24.4 °C to 29.3 °C. Differences between measured and simulated temperatures ranged from -0.9 °C to 1.2 °C with a RMSE of 0.24. The MARE between

measured and simulated water temperatures was 1.55%. Eighty nine percent of the simulated temperatures were within 1°C of the measured temperature.

The error statistics for the simulated vertical profiles of water temperature were calculated for the calibration period. The monthly goodness of-fit statistics between observed and simulated temperatures are given in Table 4.

Table 4 - Goodness-of-fit statistics between observed and simulated temperatures during the calibration period for the Victoria reservoir

	Calibration year 1995												
	Jan 9	Feb 1	Mar 2	Apr 28	May 8	Jun 8	Jul 11	Aug 9	Sep 26	Oct 12	Nov 10	Dec 19	Mean
RMSE (\pm °C)	0.001	0.145	0.057	0.318	0.422	0.313	0.228	0.243	0.251	0.364	0.428	0.158	0.244
MRAE (%)	0.026	1.367	0.807	1.964	2.157	1.800	1.647	1.525	1.553	2.119	2.308	1.367	1.553

4.6 Verification of the DYRESM

To verify the accuracy of the parameters of the model calibrated based on the data in the year 1995, the Victoria reservoir was simulated for the period January 17th through December 31st, 1996.

Simulated water temperatures in 1996, using the same parameter values obtained from the 1995 calibration, were very similar to measured temperatures.

Figure 4 presents the comparison of all observed water temperatures (86 observations) for January through December 1996 with corresponding simulated values for St 2. Observed water temperatures in 1996 ranged from 23.6 to 28.7°C. Differences between observed and simulated temperatures ranged from -1.58 to 1.08°C with a RMSE of 0.24. The MRAE between measured and simulated water temperature was 1.55%, indicating a good calibration of the model. Ninety one percent of the simulated temperatures were within 1°C of the measured temperature. Simulated water temperatures during the 1996 verification period, like the 1995 calibration period, provided an excellent simulation of water temperature in the Victoria reservoir with most simulated values within plus or minus 1°C of the observed value.

The fit statistics were calculated for the verification period, too. The monthly goodness of-fit statistics between observed and simulated temperatures are given in Table 5.

4.7 Application of the model

The calibrated hydrodynamic model (DYRESM) was used to run different operational scenarios which are useful to make decisions for improving water quality in the Victoria reservoir. Simulations were developed to evaluate the stratification cycle during a period of 3 years. Impact of withdrawal quantity and withdrawal level on stratification in the reservoir was investigated based on the model.

4.8 Simulation for a 3 years period

After verification, the calibrated DYRESM model was run for a period of three years from 1997 to 1999 to study the stratification in the Victoria reservoir. Initially, historical releases were used in the simulation. Figure 5 (a) shows the resulted distribution of water temperature in the reservoir during that period.

The results show that the water temperature varied annually, seasonally and spatially in the Victoria reservoir. Thermal stratification is strong during the warm period approximately from March to August. During the warm period in 1997 and 1999 water temperatures range from around 29°C at the surface to nearly 25°C at the deeper levels. Surface water temperature is about 31°C for the period May-June in 1998. During the cold period (approximately from October to February) the reservoir water gets mixed and top to bottom temperature vary from 26°C to 25°C only.

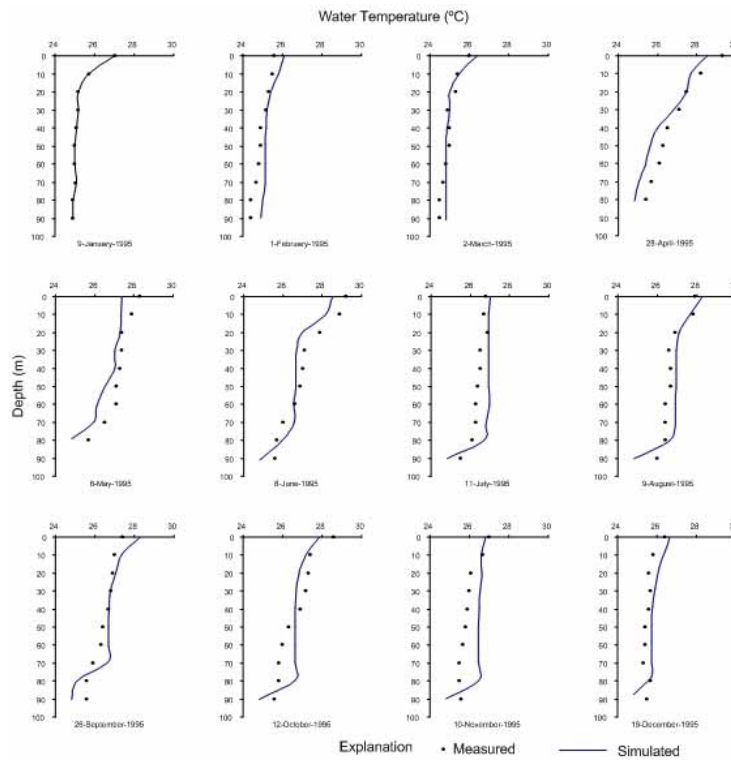


Figure 3 - Measured and simulated vertical profiles of water temperature at Victoria reservoir St 2, during 1995

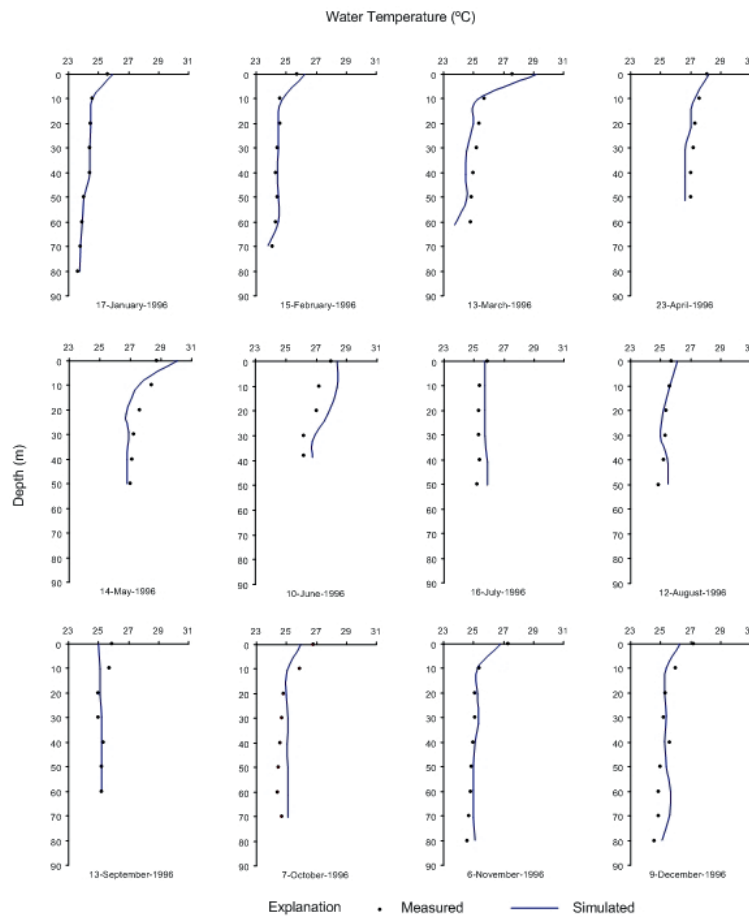


Figure 4 - Measured and simulated vertical profiles of water temperature at Victoria reservoir St 2, during 1996

Table 5 - Goodness-of-fit statistics between observed and simulated temperatures during the verification period for the Victoria reservoir

	Verification year 1996												
	Jan 17	Feb 15	Mar 13	Apr 23	May 14	Jun 10	Jul 16	Aug 12	Sep 13	Oct 7	Nov 6	Dec 9	Mean
RMSE (\pm °C)	0.013	0.060	0.700	0.151	0.554	0.541	0.211	0.129	0.181	0.347	0.077	0.305	0.272
MRAE (%)	0.198	0.762	2.816	1.330	2.260	2.537	1.693	1.241	1.087	2.169	0.944	1.877	1.576

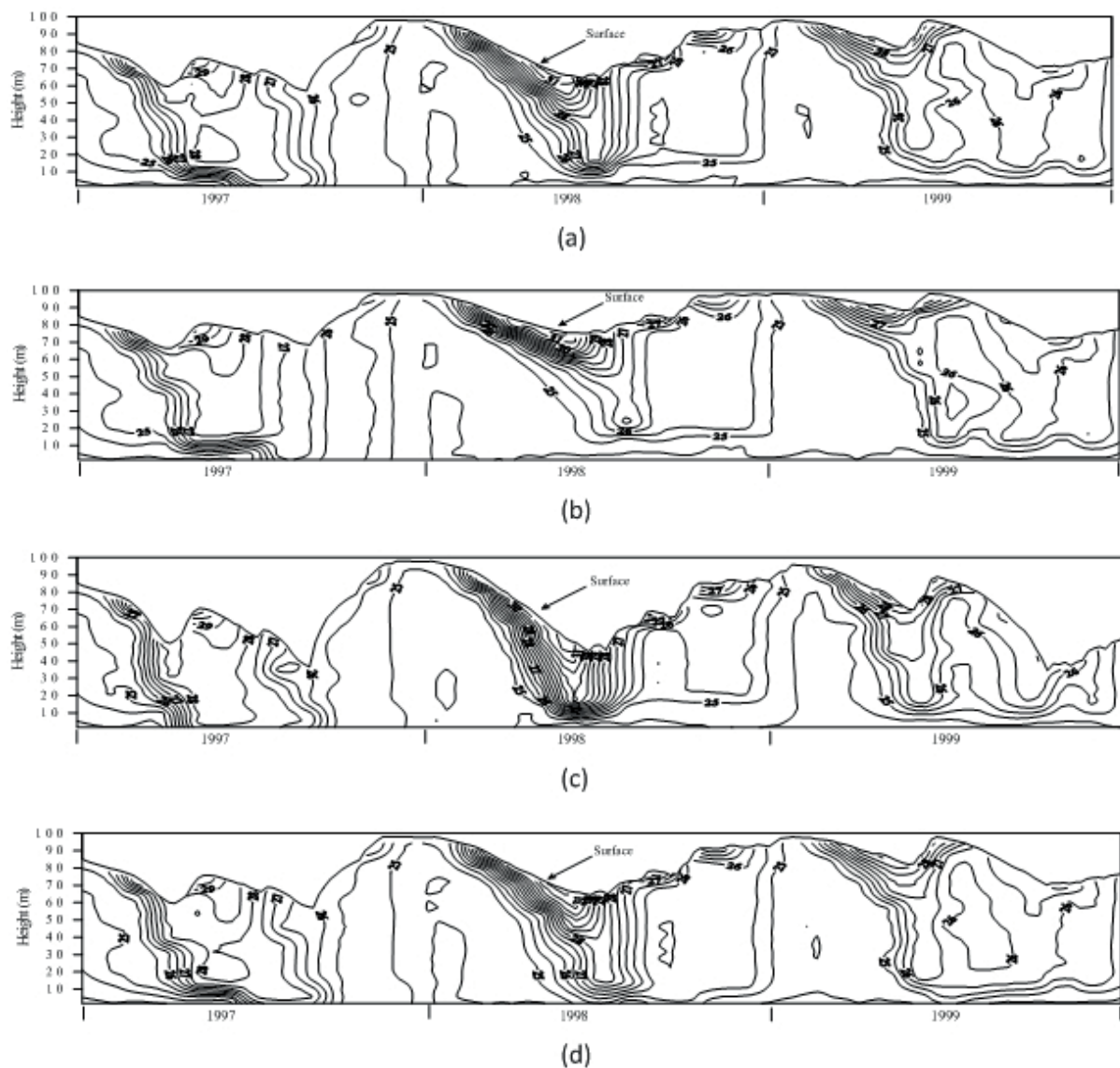


Figure 5 - Distribution of water temperature in the Victoria reservoir St 2, from January 1997 to December 1999: (a) Historical operation, (b) Release quantity reduced, (c) Release quantity increased, and (d) Release from outlets at different levels.

4.9 Impact of the withdrawal quantity

Reservoir release quantity has an impact on thermal stratification. Reservoir behaviour was studied with a different reservoir release pattern using two simulations. In the first, the release from the upper outlet was decreased by

25% and in the second, the release was increased by 25% for the period from March to May (at the onset of stratification period) in all the three years. Note that the dam has two outlets at different levels. The release during the other period was kept unchanged. Figures 5

(b) and (c) show the resulted distributions of water temperature.

The results clearly indicate that the thermal stratification is affected by the change in the release quantity. When release quantity was decreased by 25% reservoir stratification has slightly decreased. However, the stratification has slightly increased when the release quantity was increased by 25%. This suggests the possibility to change the strong stratification in the Victoria reservoir by manipulating the releases.

4.10 Simulation of impact of the withdrawal level

Impact of the outlet elevation on the thermal stratification and thus on water quality was studied next. For that, 75% of water was withdrawn from the upper outlet (15 m above the bottom) and 25% from lower one (8.2 m above the bottom) during the onset of stratification period, March to May, in all the three years. Total release was made through the upper outlet during the balance period. Figure 5 (d) shows the resulted distributions of water temperature. The results indicate that the outlet elevation affects the thermal stratification in the reservoir. The thermocline has become deeper when water is released through both outlets. The surface temperature has not changed, but the bottom water temperature has improved considerably. Besides, stratification is observed to be reduced significantly. Releasing from the bottom outlet (at the onset of the warm period), where water is found to be stratified is observed to be a good operation pattern to improve water quality in the reservoir. This suggests the possibility to decrease strong stratification in the Victoria reservoir by manipulating releases.

5. Conclusions

A one-dimensional hydrodynamic model, DYRESM, was calibrated and verified for the simulation of thermal stratification of the Victoria reservoir in Sri Lanka. The model predicted thermal stratification in the reservoir with fair precision. Predictions of the onset of stratification, surface temperature, hypolimnetic temperature and mixed-layer depths were all in agreement with the observations. The quantitative and qualitative criteria of model prediction showed that the model could simulate the annual dynamics

reasonably well. The Victoria reservoir was observed to be thermally stratified during the warm periods of the year.

The model enables the prediction of thermal stratification in the reservoir body using data that can be collected easily, such as climatological data and reservoir inflow quantity and quality. This could avoid continuous expensive reservoir water quality monitoring programmes.

The three year long (1997-1999) simulation showed that the annual cycle of stratification clearly. Since thermal stratification in a reservoir determines the water quality in a reservoir body, the model enables predicting adverse effects with respect to water quality in the reservoir. In such situations, reservoir managers will be able to take precautionary measures by controlling stratification in the reservoir by manipulating withdrawals. The study, based on two different withdrawal patterns, has shown that stratification in the Victoria reservoir could be altered by manipulating the withdrawal. Thus, the impact of many alternative operational patterns on thermal stratification in the reservoir could be studied with the help of the model in advance to avoid adverse water quality conditions in the reservoir as well as supplied from the reservoir.

Results from this study will provide reservoir management with information to better understand how changes in hydrology and water quality in the basin affects water quality in the reservoir. With this information, managers will be able to more effectively manage their reservoir.

Acknowledgements

National Science Foundation, Sri Lanka for providing financial assistance through its research grant RG 2001/E01, Headworks Administration, Operation and Maintenance unit of the Mahaweli Authority of Sri Lanka and Natural Resource Management Centre at Peradeniya, Sri Lanka for providing data and Centre for Water Research, University of Western Australia for giving permission to use the DYRESM model are greatly acknowledged.

References



1. Abeysinghe, K.G.A.M.C.S., Nandalal, K.D.W. and S. Piyasiri (2005) "Prediction of thermal stratification of the Kotmale reservoir using a hydrodynamic model", *Journal of the National Science Foundation of Sri Lanka*, Vol.33, No.1, pp.25-36.
2. Allen, R.G., Pereira, L.S., Raes, D. and M. Smith (1998) "*Crop evapotranspiration – Guidelines for computing crop water requirements*", FAO Irrigation and drainage paper 56, FAO, Rome.
3. Antenucci, J.P., Alexander, R. Romero, J.R. and J. Imberger (2002) "Management strategies for a eutrophic water supply reservoir – San Roque, Argentina", Proceedings of IWA 3rd World Congress, Australia.
4. Campos, H., Hamilton, D.P., Villalobos, L. Imberger, J. and A. Javan (2001) "A modelling assessment of potential for eutrophication of lake Rinihue, Chile", *Arch. Hydrobiology*, pp.101-125.
5. Dake, J.M.K. and D.F.R. Harleman (1969) "Thermal stratification in lakes-analytical and laboratory Studies", *Water Resources Research*, 5, 484-495.
6. Gal, G., Parparvo, A., Wagner, U. and T. Rozenberg (2003) "Testing the impact of management scenarios on water quality using ecosystem model", Annual report to Israel Water Commission, pp.215.
7. Hamilton, D. P. and S.G. Schladow (1997) "Prediction of water quality in lakes and reservoirs. Part I. Model description", *Ecological Modeling*, 96, 91-110.
8. Hostetler, S.W. and P.J. Bartlein (1990) "Simulation of lake evaporation with application to lake level variations of Harney-Malheur, Oregon", *Water Resources Research*, Vol.26, No. pp.2603-2612.
9. Huber, W. C., Harleman, D. R. F. and P.J. Ryan (1972) "Temperature prediction in stratified reservoirs", *Journal of Hydraulics Division, ASCE*, 98, 645-665.
10. Imberger, J. (1981) "The influence of stream salinity on reservoir water quality", *Agricultural water management*, Vol.4, pp.255-273.
11. Imberger, J., Patterson, J. C., Hebbert, B. and I.C. Loh (1978) "Dynamics of Reservoir of Medium Size", *Journal of the Hydraulic Division, ASCE*, 104(HY5), 725-743.
12. Imberger, J. and J.C. Patterson (1981) "A dynamic reservoir simulation model-DYRESM", 5, in H.B. Fisher (ed), *Transport Models for Inland and Coastal Waters*, Academic Press Inc., New York, USA, pp.310-361.
13. Joehnk, K.D. and L. Umlauf (2001) "Modeling the metalimnetic oxygen minimum in a medium sized alpine lake", *Ecological Modeling*, Vol.136, pp.67-80.
14. Lam, D.L.C., Schertzer, W.M. and A.S. Fraser (1983) "Simulation of Lake Eire Water Quality Responses to Loading and Weather Variations", *IWD Scientific Series No.134*, National Water Research Institute, Canada Centre for Inland Waters, Burlington, 232p.
15. Markofsky, M. and D.R.F. Harleman, D.R.F. (1973) "Prediction of Water Quality in Stratified Reservoirs", *Journal of the Hydraulic Division, ASCE*, 99(HY5), 729-745.
16. Nandalal, K.D.W. (1995) "Reservoir Management Under Consideration of Stratification and Hydraulic Phenomena", *PhD Dissertation*, Department of Water Resources, Wageningen Agricultural University, The Netherlands.
17. Nandalal, K.D.W., Abeysinghe, K.G.A.M.C.S. and S. Piyasiri (2005) "Improvement of Water Quality in a Reservoir: Case of Kotmale Reservoir in Sri Lanka", Abstracts Volume, 11th World Lakes Conference, Nairobi, Kenya, p.26.
18. O' Connor and D.J. Mueller (1970) "A Water Quality Model of Chloride in Great Lakes", *Journal of the Sanitary Engineering Division, ASCE*, Vol.96, No.SA4, August, pp.955-975.
19. Orlob, G. T. (1983) "Mathematical modeling of water quality: streams, lakes and reservoirs", In: Orlob, G. T. (Ed.).

Series on Applied System Analysis. Wiley
IIASA, Inter.

20. Patterson, J. C., Hambling, P. F. and J. Imberger (1984) Classification and dynamic simulation of the vertical density structure of lakes, *Limnological Oceanography*, **29**, 845-861.
21. Piyasiri, S. (1991) "Limnology project at Mahaweli Reservoirs, Some properties of Kotmale, Victoria and Randenigala reservoirs", *Vidyodaya Journal of Science*, Vol. 3 No. 1, pp. 45-61.
22. Piyasiri, S. (1996) "The Chlorophyll-a content, species composition and population structure of phytoplankton in Randenigala reservoir in Sri Lanka", *Vidyodaya Journal of Science*, Vol. 5. No.1, pp. 29-41.
23. Rounds, S.A. and T.M. Wood (2001) "Modeling water quality in the Tualatin River, Oregon, 1991-1997", *Water-Resources Investigations Report 01-4041*.
24. Samuel, T.D.M.A. (2000) "Solar radiation distribution over Sri Lanka", *Bulletin No.1, Solar Research Laboratory*, University of Peradeniya, Sri Lanka.
25. Spigel, R.H. and D.J. Ogilvie (1985), "Importance of selective withdrawal in reservoirs with short resident times: A case study", *Proceedings of the 21st IAHR Congress, Melbourne, Australia*, pp.275-279.



An Approach to Grade Aggregates having Mild Potential Alkali - Silica Reactivity

C.K. Pathirana, H. Abeyruwan, H.M.G.T.A Pitawala and A.P.N. Somaratna

Abstract: In many parts of the world concrete structures have failed due to Alkali-Aggregate Reaction (AAR). Researchers have explored remedial actions to be taken and mitigation techniques to be followed in concrete construction to alleviate the problem of AAR. In Sri Lanka, so far no documented evidence has been produced about investigations of this nature though there are a few old concrete structures which are still being used but showing symptoms similar in nature to AAR. To investigate the potential alkali-silica reactivity of Sri Lankan aggregates, preliminary work has been attempted. A quick chemical method which is used in many countries has been used to test fine and coarse aggregates collected from different locations in the country. According to the results, many aggregates can be placed in the non-reactive zone of the chart of innocuous and deleterious aggregates illustration of ASTM C 289. But some fall in a gray area close to the boundary of the demarcation of reactivity, which could be defined as a 'slowly reactive' zone. Having recognized the significance of quantifying the degree of reactivity of such slowly reactive aggregates, a new parameter called 'potential reactivity index' has been introduced. This index may serve the process of screening aggregates for structures of long life expectancies.

Keywords: Alkali-Aggregate Reaction, slowly reactive aggregates, potential reactivity index

1. Introduction

Concrete has become a widely used construction material all over the world. One of the major causes of serviceability and durability problems of concrete structures is the Alkali-Aggregate Reaction (AAR), which can lead to premature cracking and distortion of the structures. In general terms it is a reaction between aggregates and the alkalis in the pore water in cement paste. Literature [1, 2, 3] has shown that AAR can be separated into two main categories according to the active mineral component of the aggregate which is involved in the reaction. When this active mineral component is silica, the reaction is called Alkali-Silica Reaction (ASR) and when it is carbonates, the reaction is called Alkali-Carbonate Reaction (ACR). According to the literature [2, 3], ASR is more common than ACR. All aggregates containing silica or carbonates are not equally susceptible to AAR. In the early 1940's, the first evidence of AAR was reported by Stanton [4] as formation of cracks in some concrete pavements in California, USA. The cause of these cracks had been identified as the formation of a gel layer due to high alkali cements and some mineral phases in certain types of aggregates. With the absorption of water, this layer of gel expands. As a result there may be expansion, cracking, increased permeability, and decreased

modulus and tensile capacity of concrete [5]. However cement is not always the only source of the alkalis involved in the deleterious reactions. Deleterious alkalis may come from groundwater, seawater, deicing chemicals, or other sources (eg. aggregates) [6]. The identification of AAR as a cause of concrete deterioration needs an integration of field and laboratory evidence. It is highly complicated and costly to contain the reaction once it starts. There are various engineering standards for the ingredients to meet before being used in concrete construction. Screening of reactive aggregates is an appropriate method of avoiding long-term problems of AAR.

Special attention must be paid to aggregates as the performance characteristics in the durability of the structure depend on their mineralogy and texture.

Eng. C K Pathirana, AMIE (Sri Lanka), BScEng. Peradeniya, MScEng. Peradeniya, Lecturer, Dept. of Civil Engineering, University of Peradeniya.
H Abeyruwan, C Eng., MICE, MIE Aust., CP Eng., BScEng. Sri Lanka, MPhil. (Hong Kong), Senior Lecturer, Dept. of Civil Engineering, University of Peradeniya.
Eng. (Dr) A P N Somaratna, MIE (Sri Lanka), C Eng., BScEng Sri Lanka, M.S. (Illinois), PhD (Illinois), Senior Lecturer, Dept. of Civil Engineering, University of Peradeniya.
Dr. H M G T A Pitawala, BSc (Special) Peradeniya, MPhil, Peradeniya, Ph.D. Germany, Senior Lecturer, Dept. of Geology, University of Peradeniya.

To investigate the potential alkali-silica reactivity of aggregates, the American Society for Testing and Materials (ASTM) C 289 method, a rapid chemical test, has been widely used all over the world. The aggregates are categorized as deleterious, potentially deleterious and innocuous by this standard test. In literature, it has been reported that in some cases though the aggregates were classed as non-reactive or uncertain by standard methods, the structures made out of such aggregates had shown the effects of AAR [7, 8]. Over the past seventy years, many researchers [1 – 5] have carried out a fair amount of work on this subject. Some have indicated that the current standard test methods used are not stringent enough to identify certain levels of the reactivity [8]. In Sri Lanka too, there are large concrete structures such as dams about 20 years old. Those may also be susceptible to AAR though no such complications have been documented yet. The objective of this study is to propose a test method and graded reactivity level for identification of reactive aggregates in Sri Lanka.

Several samples of aggregates were collected from a few locations in the country and tests were carried out to determine the reactivity level. In compliance with ASTM C 295, petrographic examination of aggregates was also performed to identify any reactive components of aggregates which could induce expansive alkali-aggregate reaction.

2. Sample collection and Method of Study

Locations of samples were selected randomly in the region shown in Figure 3 for initiation of the research study. Samples of coarse aggregates and fine aggregates were collected from active quarries in Gampola, Peradeniya, Kothmale, Rikillagaskada, Mahiyangana, Thalawakele, Nuwaraeliya, Padukka, Horana, Aladeniya, Kaduwela, Watagoda, Nillambe, Welioya, Sarasavigama, Haragama, Dambadeniya and Oluvil.

Further investigations will also be carried out in order to identify the supply chain of the aggregates to construction sites. This will provide us a meaningful strategy to investigate for AAR the structures built with such aggregates.

3. Experimental Procedure

The standard test ASTM C 289 – 07 [9] was the basis of this study. This test method covers chemical determination of the potential reactivity of an aggregate with alkalis and it is fairly quick. Using this test, the potential alkali-silica reactivity of these aggregates was investigated.

Thin sections were also prepared from aggregate samples for the petrographic examination according to ASTM C 295 – 08 [10].

3.1 Preparation of test samples

3.1.1 Reaction samples

300 g sample was sieved through a set of sieves ranging from aperture size 300 μm to 150 μm , discarding all material that passes the 150 μm sieve. Then the sample (in small portions) was crushed and ground using a disk pulverizer, mortar and pestle. Grinding was continued until the amount of material passing through the 300 μm sieve and remaining on the 150 μm sieve was about 110 to 150 g. To ensure that all material finer than the 150 μm sieve has been removed, the sample was washed over a 150 μm sieve. The portion retained on the 150 μm sieve was taken as the test sample.

3.1.2 Mineralogical studies

50 μm thick slices were cut from the aggregate samples and thin sections were prepared from them at the Department of Geology, University of Peradeniya. Samples of fine aggregates were mounted on glass slides. Primary and secondary minerals in the samples were identified using optical microscopes.

3.2 Methodology

3.2.1 Reactivity test

Three representative 25.00 ± 0.05 g portions of a test sample were weighed. Each portion was placed in three stainless steel reaction containers and 25 ml of 1.000 N NaOH solution was added to each by means of a pipet. 25 ml of the same NaOH solution was poured into a fourth reaction container to serve as a blank. Following the procedure given in ASTM C 289 – 07, filtrates were prepared. Then a diluted solution was



prepared from the filtrate to determine the dissolved silica and the reduction in alkalinity. In this study, the gravimetric method was selected to measure dissolved silica. Using titrations with 0.05N HCl to the phenolphthalein end point, reduction in alkalinity was calculated. The same procedure was followed for all the aggregate samples.

4. Experimental Results

4.1 Reactivity Tests

Table 1 shows the values obtained for dissolved silica, S_c , and the reduction in alkalinity, R_c , for tested samples. According to ASTM C 289 the determination of reactivity is made by considering the location of each sample on a plot of reduction in alkalinity vs. dissolved silica. Figure 1 shows the three zones in the plot. However it is felt that it is unrealistic to expect sharp boundaries among the zones. In this study new parameters are proposed to take into account the gradual transition between zone 1 and zone 2/3. The minimum distance from a position within zone 1 in the plot to the zone boundary has been named as the 'potential inertness index', d , estimated in natural scale and not in log scale (see Figure 1). The 'potential reactivity index' (PRI) has been defined as follows.

$$PRI = 100/(1 + d) \quad \dots\dots(1)$$

This new concept is proposed to quantify the potential reactivity of the materials which are categorized as innocuous according to the current standard tests but marginally reactive. PRI is defined in such manner that when d equals zero the index becomes 100% and the material belongs to reactive category. As d increases the index becomes smaller which means that the material has a lower relative potential reactivity.

Both these parameters were estimated for each sample in this study (Table 1).

Figure 2 shows the potential reactivity of samples tested according to the standard test ASTM C 289 and Table 1 lists their Potential Reactivity Indices. Figure 3 shows their geographic distribution.

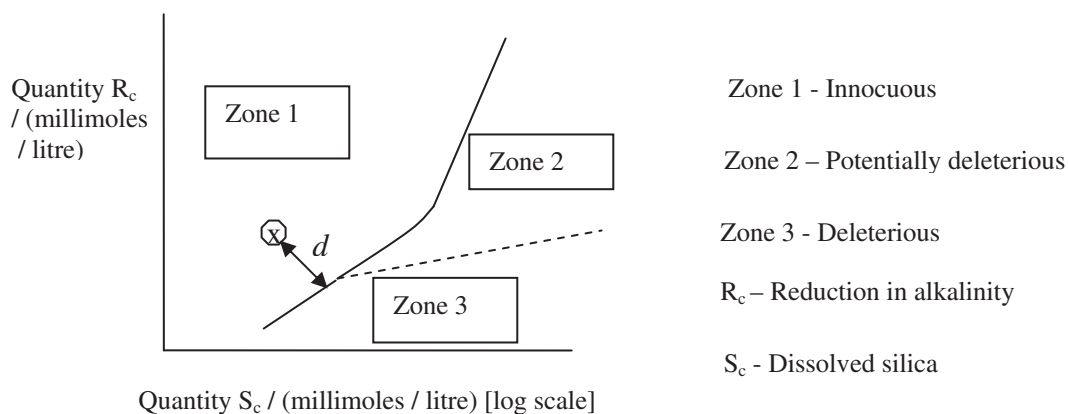


Figure 1 - Illustration of Potential inertness index of a sample aggregate

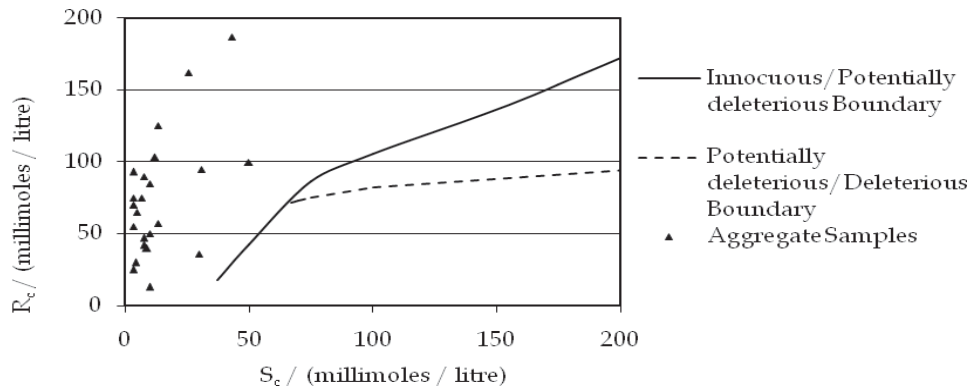


Figure 2 - Potential Reactivity levels of samples according to ASTM C 289

Table 1 - Reduction in alkalinity and dissolved silica for aggregate from different locations

Location	Reduction in alkalinity, R_c / (millimoles / litre)		Dissolved silica, S_c / (millimoles/ litre)	Potential Inertness Index ¹ 'd' (millimoles/ litre)	Potential Reactivity Index (PRI) %
	Crushed rock	Natural uncrushed sand			
Gampola	65		5.00	50.0	1.96
Kaduwela	25		3.33	39.6	2.46
Thalawakele (tunnel muck)	55		3.33	48.1	2.04
Watagoda	75		3.33	55.3	1.78
Kothmale (switchyard)	125		13.32	72.0	1.37
Rikillagaskada	93		3.33	63.1	1.56
Nillambe	50		10.00	40.2	2.43
Thalawakele	187		43.30	97.4	1.02
Padukka	40		8.88	38.2	2.55
Horana	42		7.77	39.9	2.44
Welioya	70		3.33	53.4	1.84
Niyangamdora	70		3.33	53.4	1.84
Galaha	90		7.66	57.9	1.70
Sarasavigama	47		7.75	41.4	2.36
Dambadeniya	75		6.66	52.3	1.88
Aladeniya	30		4.44	39.8	2.45
Haragama	36		30.00	16.8	5.62
Kothmale		162	25.50	88.5	1.12
Oluvil		13	9.99	30.4	3.18
Nuwara Eliya		57	13.50	39.2	2.49
Mahiyangana		103	12.20	60.3	1.63
Peradeniya		95	30.80	40.3	2.42

¹ 'd' is in natural scale.



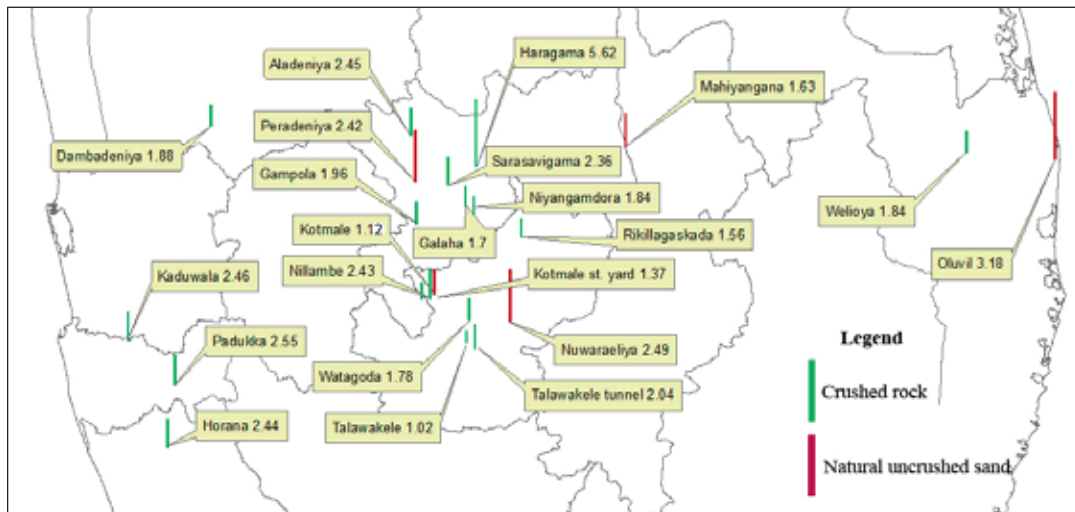


Figure 3 - Potential Reactivity Index of aggregates and their locations

Table 2 - Summary of petrographic studies

Sample No.	Texture	Angular grains
S-5	Mineralogy	Quartz, feldspar and biotite
from Haragama	Secondary Mineralization	Both amorphous and crystalline bladed phases are present. Micro crystalline products along the fractures and the cleavages of minerals were identified.
Sample No.	Texture	Fine to medium grained angular particles.
S-7	Mineralogy	Quartz and opaque minerals
From Galaha	Secondary Mineralization	Alterations are present. Micro-crystalline materials are also present in cracks that intersect each other. However, the intensity of the alteration is not considerable. Some voids of grains were filled by secondary iron products.
Sample No.	Texture	Angular coarse to medium grained.
S-8	Mineralogy	Most of grains are fresh (90 percent) quartz, garnet, iron oxide minerals (magnetite and ilmenite) and biotite.
From Sarasavigama	Secondary Mineralization	Alteration of biotite into muscovite is present. Weakly developed recrystallizations along fractures of quartz grains are found from few grains. The cracks of most of grains are lacking of secondary mineralization.

4.2 Petrography

Petrographic studies revealed the presence of both stable minerals and unstable minerals in aggregates. They can also be used to identify some secondary minerals (altered minerals) which may have formed by chemical reactions developed under natural conditions. The textural and mineralogical characteristics of aggregates can be used to recognize any deleterious components present and to classify them. Generally, the natural silica constituents such as opal, chalcedony, quartz, cristobalite,

tridymite, chert are considered to be potentially reactive [8]. Table 2 summarizes the results of petrographic examination of some of the samples.

5. Discussion

The phenomenon of ASR is complex, and there are many interacting and interdependent parameters that influence its occurrence. Many countries have experienced ASR which results in unpredictable and uncontrollable effects on concrete structures. Therefore, it is very important to assess and evaluate the potential

reactivity of aggregates prior to their use in concrete construction.

The structure and texture of siliceous fractions are generally described in terms such as amorphous, cryptocrystalline, microcrystalline and crystalline. Silica (SiO₂) itself occurs in a number of polymorphic forms. The most common form of silica minerals includes quartz, tridymite, cristobalite, opal and chalcedony group, which covers a number of varieties of silica, composed of minute crystals of quartz with submicroscopic pores.

Microscopic investigations indicated that almost all studied aggregates have primarily (fresh) quartz as major mineral constituent with angular texture. However some samples collected from Haragama are characterized by amorphous phases developed recently. This is of vital importance in recognizing the susceptibility of potential reactivity as many reactive aggregates contain amorphous phases according to previous studies [7].

Results of the alkali-reactivity tests for aggregate samples have been shown in Table 1. Though the results of ASTM C 289 test for all samples fall in the region of 'innocuous', it may not be treated as a definitive criterion for acceptance of an aggregate to be used in concrete structures of long service life expectancy, as slowly reactive aggregates might escape detection [7]. In the case of a sample falling close to the innocuous/deleterious boundary the potential reactivity value (PRI) may give some indication of reactivity. The higher the potential reactivity index, the closer the sample is to the zone of potentially deleterious or deleterious zone. With the continuation of data a gray area close to the boundary of the demarcation of reactivity could be defined as a 'slowly reactive zone'. Table 2 shows that Haragama sample has an index of 5.62 which is very close to the boundary of zone 3 where aggregates are considered deleterious. Even though there is a possibility of determining the potential reactivity of an aggregate by petrographic examination, it does not give any measure of the degree of reactivity, and there should be some ancillary testing to confirm it.

Acknowledgement

Financial support provided by UGC grant No. UGC/ICD/RPC/015 to the first author and NSF grant No. RG/2007/E/06 to the fourth author is gratefully acknowledged.

References

1. ACI Committee 221, *State-of-the-Art Report on Alkali-aggregate Reactivity (221.1R-98)*, American Concrete Institute, Farmington Hills, Michigan, USA, pp.1-31, 1998.
2. Xiangyin Mo, ChenjienYu and Zhongzi Xu, *Long-term Effectiveness and Mechanism of LiOH in inhibiting Alkali-Silica Reaction*, Cement and Concrete Research, 33, pp. 115-119, 2003.
3. Xiangyin Mo, Tongshun Jin, Gang Li, Keyu Wang, Zhongzi Xu and Mingsho Tang, *Alkali-Aggregate Reaction suppressed by Chemical Admixture at 80 °C*, Construction and Building Materials, 19, pp. 473-479, 2005.
4. Stanton, T. E., *Expansion of Concrete through Reaction between Cement and Aggregate*, ASCE Proceedings, 66, No.10, pp. 1781-1811, 1940.
5. Chen, J., Jayapalan, A. R., Kim, J. Y., Kurtis, K. E. and Jacobs, L. J., *Nonlinear Wave Modulation Spectroscopy Method for Ultra-Accelerated Alkali-Silica Reaction Assessment*, ACI Materials Journal, pp. 340-348, July – August, 2009.
6. FHWA-HRT-04-150, *Petrographic methods of examining hardened concrete: A petrographic manual*, Virginia Transportation Research Council, VA, 2004, pp. 155-179.
7. Shayan, A. and Quick, G. W., *Microscopic Features of Cracked and Uncracked Concrete Railway Sleepers*, ACI Materials Journal, pp.348-361, July – August, 1992.
8. Swamy, R. N., *The Alkali-Silica Reaction in Concrete*, Blackie and sons Ltd., Glasgow and London, 1992, Ch. 3.
9. American Society for Testing Materials, ASTM C 289 – 07, *Annual Book of ASTM Standards, Concrete and Aggregates*, Vol. 04.02, pp. 179-185, 2009.
10. American Society for Testing Materials, ASTM C 295 – 08, *Annual Book of ASTM Standards, Concrete and Aggregates*, Vol. 04.02, pp.199-206, 2009.



Suitable Bridge Pier Section for a Bridge over a Natural River

G. A. P Gampathi

Abstract: Estimation of maximum scour depth at the bridge pier is necessary for the safety and economy of the bridge design. Therefore, the phenomenon of scour around bridge piers was extensively studied from the literature to find the effect of pier shapes and inclined flow on scour depth at bridge piers.

It was found from the analysis that scour depth increases with the increase of the flow angle relative to the pier axis, but for a cylindrical pier, maximum scour depth does not change with flow angle. When the flow angle is at 30° , the scour depth for the cylindrical pier is smaller than other pier shapes; hence circular pier shape is more suitable for natural rivers which have possibility of changing flow direction.

Keywords: Scour Bridge pier, Pier axis, Flow angle, Cylinder

1. Introduction

Scour is the local lowering of stream bed elevation which takes place in the vicinity or round a structure constructed in flowing water. Scour take placed around bridge piers, abutments, around spur, jetties and breakwaters due to modification of flow pattern in such a way as to cause increase in local shear stress. This in turn dislodges the material on the stream bed resulting in local scour. In the case of bridges, the estimation of correct depth of scour below the stream bed is very important since that determines the depth of foundation.

Hurber [1] has stated that since 1950 over 500 bridges in USA have failed and that the majority of the failures were related to the scour of foundation material. Such data are not available for the PNG (Papua New Guinea) bridges. However, it is known to all of us that longest bridge in PNG, Markham Bridge is not fully functioning due to scour and settlement of one of its major pier.

The concern about safety of bridges is primarily due to three reasons which are: 1).inadequate knowledge about scour phenomenon when the bridges were constructed; 2). inadequate data on which the design flood was chosen and 3). increase in the loading on the bridges due to increase in size of trucks and other vehicles and their frequency of operation.

The stream bed lowering at the bridge can take place due to four primary reasons. If the bridge is located downstream of a large dam, there is a slow lowering of the bed and reduction of

stream slope due to degradation. Degradation takes place when the stream transporting sediment becomes deficient in sediment supply due to sediment being stored upstream of the dam. In extreme case this lowering can be as much as 4 to 6 meters. Secondly, if for reducing the cost of the bridge the stream is contracted by building guide bunds etc..., such contraction can cause additional lowering of the stream bed.

The third type of lowering that takes place around the bridge pier is due to modification of flow structure due to presence of pier. Depending on the pier shape and free stream condition, an eddy structure comprising of one or more of the three eddy structures, namely horseshoe vortex, wave vortex and the trailing vortex system can form; which increases the local shear on the bed and causes scour. Typical formation of horseshoe vortex and wake vortex are shown in figure 1. Lastly; additional scour can also take placed if the flow direction is inclined to the pier axis.

Eng. G.A.P Gampathi, M.Eng (Singapore) , B.Sc (Hons), AMIE(Sri Lanka), Lecturer , University of Technology, Papua New Guinea.

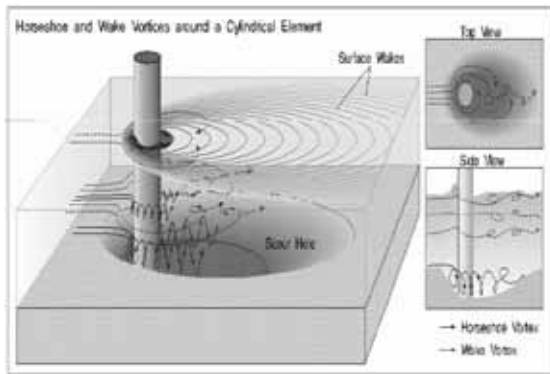


Figure 1 : Formation of Horse shoe and Wake vortices

Eventhough, number of researchers have studied the factors affecting scouring depth and hence derived formulas to evaluate the sour depth for pier. It is not considered the combined effect of flow direction and the pier shape to select an optimum section for piers.

It can be described, when the axis of the pier makes an angle θ with the general direction of the flow, two major changes take place in the flow field. Except in the case of cylindrical pier, the separation pattern is drastically changed resulting in change in vortices. Secondly, the open width between the piers, perpendicular to the flow direction reduces as the angle of inclination θ increases.

Therefore, the combined effect of pier shapes and angle of inclination of pier axis to the flow direction on scouring depth is extremely important in pier designing. Since the depth of foundation of pier decided by the maximum scour depth, the finding of this study is more important for selecting a correct pier shape to reduce the depth of scour.

Further, most of natural river banks are not stable for long times, it may change the direction of flow due to erosion. It also possible due to deposition of sediment inside the river. Therefore it is risky to select a pier section in traditional way, just thinking that the river flow is axial. Hence, it is better to select a suitable pier section for natural river by studying the effect of flow direction.

2. Literature Review

A number of papers have been published since 1940 on various aspects of scour around bridge piers. Based on the experimental work and some theoretical analysis it is found that the following factors affect the scour depth at the bridge pier.

i) Whether the incoming flow is clear water flow or it carries sediment: clear water flow

occurs when u^*/u_{*c} is less than unity while for sediment transporting flow U^*/U_{*c} is greater than unity. Here $U^* = \sqrt{gDS}$ is the shear velocity of flow and U_{*c} is the shear velocity at which bed material starts moving, D is the depth of flow in the river and S is the river slope. Average shear stress on the bed is $\tau_0 = \zeta_f U_{*se} \gamma_f DS$ where γ_f is the unit weight of water and ζ_f its mass density. All factors remaining the same clear water scour is found to be about 10 % more than scour in scour in sediment transporting flows. Further, whereas in clear water flow it takes several hours to reach the maximum scour below river bed d_{sc} , in sediment transporting flow corresponding equilibrium scour depth d_{se} is reached in relatively shorter time.

ii) Effect of change in depth of flow: experiments by Melville and Sutherland have shown that when (depth of flow/ pier width) ration i.e., D/b is greater than 2.6, scour depth does not depend on the depth of flow; for smaller depths the scour depth depends on the depth of flow.

iii) Effect of shape of pier nose: the shape of the pier nose affects the strength of horse-shoe vortex as well as the separation of the flow around the bridge pier; hence it affects the maximum scour depth. The following table 1 prepared on the basis of studies by Laursen and Toch [4], Chabert and Engeldinger [3], Garde [7], and Paintal and Garde [6], gives relative effect of pier – nose shape on the maximum scour if for cylindrical pier the maximum scour is taken as unity.

Table 1: Average values of shape coefficients (K_s)

Shape		K_s
Cylindrical		1.0
Rectangular ($l/b = 2$ to 6)		1.1 to 1.25
Lenticular ($2:1, 3:1, 4:1$)		0.93, 0.79, 0.70
Elliptical ($2:1, 3:1$)		1.0, 0.86
Joukowsky profile ($4:1, 5:1$)		1.0, 0.80
Triangular:	15° apex angle	0.45
	60° apex angle	0.75
	90° apex angle	0.88
	120° apex angle	0.94
	150° apex angle	1.0

iv) Effect of angle of inclination of pier on scour depth: In this case, two major changes take place in the flow field except in the case of



cylindrical pier, the flow separation pattern is drastically changed and secondly, the open width between the piers, perpendicular to the flow direction reduces as the angle of inclination increases.

v) Effect of opening ration on scour depth: the opening ratio α is defined as $\alpha = (B-b)/B$ where B is centre to centre spacing of the piers and b is the pier width. When b is very small compared to B , α is close to unity and flow around one pier does not affect that around the other. However, as α decreases, the interference affect becomes more pronounced and scour depth increases; in such a case D_{se}/D or $D_{sc}/d \propto \alpha^{-n}$. Here D_{se} and D_{sc} are scour depths below the water surface for sediment transporting and clear water flows respectively. The analysis of extensive data collected by Garde [8] indicate that $n = 0.30$.

vi) Effect of bed material characteristics: in the case of non cohesive materials, the characteristics of bed material that affect the scour depth are sediment density, median size d of the bed material, its standard deviation and stratification. For all practical purposes the density of natural sediments can be taken as 2.65, a constant value.

As regard the sediment size, lacey-inglis approach suggests that $D_{se} \approx d^{-1/6}$. Since the average shear stress on the bed ($= \gamma_f DS$) at which bed material moves-known as the critical shear stress-increases as the sediment size increases, it stands to reason that scour depth should be affected by the size of the bed material. Hence, for given flow condition, larger than the sediment size d , smaller should be the scour depth. The clear water scour depth should decrease with increase in sediment size. Analysis of data over large of sediment size by Kothyari [9,10] has indicated that $d_{sc} \approx d^{-0.31}$ while for sediment transporting flow $d_{se} \approx d^{-0.07}$. Here d_{sc} and d_{se} are the scour depths below general bed level for sediment transporting and clear water flows respectively.

The effect of size distribution of the bed material on the scour depth is more significant. When the standard deviation σ_g of the bed material is large and the bed material contains some nonmoving sizes for a given discharge, the coarser material would tend to accumulate in the scour hole and inhibit further development of scour depth. Hence for the same median size, scour depth will be smaller for material with larger geometric standard deviation σ_g . Here

$\sigma_g = \frac{1}{2} (d_{84}/d_{50} + d_{50}/d_{16})$ and , d_{84} , d_{50} and d_{16} are such sizes that 84%, 50% and 16% material is finer than d_{84} , d_{50} and d_{16} sizes respectively.

The percentages 84 and 16 are such that for normal or Gaussian distribution $d_{84} = (d_{50} + \text{standard deviation})$ and $(d_{16} = d_{50} - \text{standard deviation})$ if the correction factor K_G is defined as

$K_G = \frac{\text{Equilibrium scour depth for non-uniform material}}{\text{Equilibrium scour depth for uniform material of the same median size}}$

K_G would depend on σ_g . On the basis of experiment data of Raudkivi [11] and Kothyari [10] the following table is given.

Table 3: Variation of K_G with σ_g

σ_g	1.0	1.5	2.0	2.4	2.75	3.3
K_G	1.0	0.9	0.75	0.5	0.38	0.25

Vii) Stratification: Ettema [26] have studied the effect of stratification of the bed material on scour depth in case of clear water scour. It is concluded that the stratification, in which a relatively thin coarse top layer covers a thick fine bottom layer, is the critical condition. Once the top coarse layer is scoured away, scour depth will rapidly increase.

viii) Effect of flow parameters

Based on certain theoretical analysis, physical reasoning and analysis of experimental data, investigators have arrived at the basic flow parameters to which the dimensionless scour depth is related. There are equations derived by different researchers to find the scour depth, but most of this type of relationship is valid for cylindrical piers. Also these equations are valid for nearly uniform bed material. However, there are commonly used formulae to estimate the bridge pier scour depth, some of these are; Lacey-Inglis Equation, laursen-Toch Equation, Kothyari-Garde-Ranga Raju's Method and Colorado Sate University Equation. Almost all these formulae were developed based on the laboratory data. This is because the scour is a very complex phenomenon that has resulted from the interaction between the flow around a bridge pier and the erodible bed surrounding it. Based on this, only very limited attempts have been successful in modeling the scour computationally. However, the formulae and

models derived from these attempts are usually applied by the civil engineers to evaluate the depth of local scour for new bridges and existing bridges that have local scour problems.

In the earlier part of this century Lacey-Inglis analysed the data from stable irrigation canals flowing through loose noncohesive sandy material in Indo-Gangetic plain and obtained the following equations for depth (or hydraulic radius) D_{LQ} and perimeter (or width) P .

$$D_{LQ} = 0.47(Q/f)^{1/3} \text{ and}$$

$$P = 4.75 \sqrt{Q}$$

Where Q is the discharge in m^3/s , D_{LQ} and P are in m and f is Lacey- Inglis silt factor related to median size of the bed material d by the equation

$$f = 1.76 \sqrt{d}$$

d in mm . on the basis of analysis of scour data on 17 bridges in alluvial rivers in North India, Inglis found that maximum scour depth below water level, D_{se} is related to computed value of D_{LQ} as $D_{se} = K D_{LQ}$, Where K is varied from 1.7 to 2.59 with an average of 2.09. Hence according to Inglis, D_{se} is given by the equation $D_{se} = 2.0 D_{LQ}$

The equation proposed by Laursen and Toch for prediction of d_{se} is $d_{se}/D = 1.35 (b/D)^{0.70}$ and the more commonly used and cited local scour formulae, namely the Colorado State University (QSU) is described below:

$$\frac{d_s}{y} = 2.0 K_1 K_2 \left[\frac{b}{y} \right]^{0.65} F_{r1}^{0.43}$$

Where d_s is scour depth, y is flow depth at the upstream of the pier, K_1 is correction factor for pier nose shape, K_2 is correction factor for the angle of attack flow, b is the pier width and F_{r1} is the Froude number at up stream of the pier. L is the pier length. K_1 and K_2 are obtained from Table 4 and 5.

Table 4: Values of K_1 for different pier types

Type of pier	K_1
Square nose	1.1
Round nose	1.0
Circular cylinder	1.0
Shape nose	0.9
Group of cylinders	1.0

Table 5: Values of K_2 for different pier types

Angle of flow attack	K_2		
	$L/b = 4$	$L/b = 8$	$L/b = 12$
0°	1.0	1.0	1.0
15°	1.5	2.0	2.5
30°	2.0	2.5	3.0
45°	2.3	3.3	4.3
90°	2.5	3.9	5.0

It is recommended that the limiting value of d_s/y is 2.4 for $F_{r1} \leq 0.8$ and 3.0 for $F_{r1} > 0.8$.

3. Calculation of Maximum Scour

Eventhough, few acceptable equations are available to find maximum depth of scour, In this section, the most widely used Colorado State University Equation was used. Maximum scour depths were calculated for three different flow conditions with sediment size of 1mm. The flow condition were selected by referring to the local river, namely Markham River and selected three set of data as follows:

- 1) Discharge ' Q ' = 11200 m^3/s , velocity ' V ' = 5.0 m/s , mean flow depth = 4.0m.
- 2) Discharge ' Q ' = 8960 m^3/s , velocity ' V ' = 4.0 m/s , mean flow depth = 4.0m.
- 3) Discharge ' Q ' = 7168 m^3/s , velocity ' V ' = 3.2.0 m/s , mean flow depth = 4.0m.

Further, in the first part of the calculation, four different pier shapes were considered to find the effect of pier shape on scour depth. In the second part of the calculation, effects of flow directions were considered.

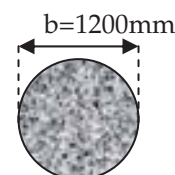
3.1 First Part of Calculation

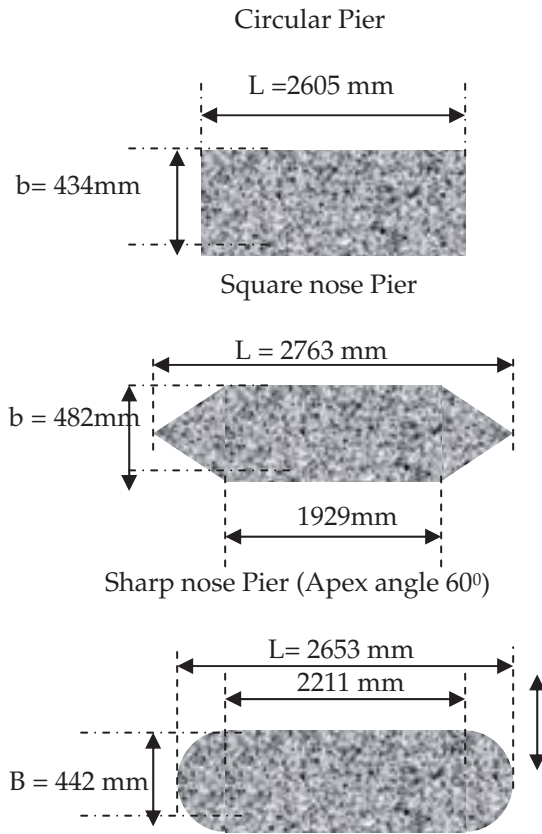
Colorado state university equation

$$\frac{d_s}{y} = 2.0 K_1 K_2 \left[\frac{b}{y} \right]^{0.65} F_{r1}^{0.43}$$

was used to

calculate the maximum scour depth for the following pier shape which are having same cross sectional areas. The results are given in table 6.





Round nose Pier
Figure 2: Pier Shapes

Table 6: Maximum depth of scour for axial flow

Pier Shape	Maximum Scour Depth / m		
	Flow condition 1	Flow condition 2	Flow condition 3
Circular	3.32	3.02	2.74
Square nose	1.72	1.56	1.41
Sharpe nose	1.65	1.50	1.36
Round nose	1.74	1.58	1.43

3.2 Second Part of Calculation

Data from table 4, 5 and 6 were used to calculate the scour depth for angular flow attack and results are given in table 7 to 9.

Table 7: Maximum depth of scour variation with flow angle for flow condition 1

Flow angle (θ)	Maximum Scour Depth / m			
	Circular	Square nose	Sharp nose	Round nose
0 ⁰	3.32	1.72	1.65	1.74
15 ⁰	3.32	3.01	2.90	3.05
30 ⁰	3.32	3.81	3.71	3.92
45 ⁰	3.32	4.82	4.62	4.87

Table 8: Maximum depth of scour variation with flow angle for flow condition 2

Flow angle (θ)	Maximum Scour Depth / m			
	Circular	Square nose	Sharp nose	Round nose
0 ⁰	3.02	1.56	1.50	1.58
15 ⁰	3.02	2.73	2.63	2.77
30 ⁰	3.02	3.51	3.38	3.56
45 ⁰	3.02	4.37	4.2	4.42

Table 9: Maximum depth of scour variation with flow angle for flow condition 3

Flow angle (θ)	Maximum Scour Depth / m			
	Circular	Square nose	Sharp nose	Round nose
0 ⁰	2.74	1.41	1.36	1.43
15 ⁰	2.74	2.47	2.38	2.50
30 ⁰	2.74	3.17	3.06	3.22
45 ⁰	2.74	3.95	3.81	4.00

4. Results and Discussion

It can be seen from the table 6 that maximum scour depth varies with the pier shape eventhough the flow and sediment conditions are equal. These results are in comparable nature since all the pier sections have equal cross sectional areas. Therefore, it can be stated that maximum scour depth occurs when the pier shape is cylindrical. Also it can be concluded that minimum scour occur when the pier shape is sharp nose. The depth of scour is decreased with flow velocity decreases, while maintaining the maximum scour and minimum scour at circular and sharp nose respectively. On the other hand, it can be seen from the reading at table 7 to 9 that scour depth

increases with the increase of the flow angle. But, the scour depth for cylindrical pier does not change with the flow angle. This is due to the flow properties and geometrical properties of cylinder are not changed with the direction of the flow. But in other cases it will increase due to modification of flow properties and contraction of flow due to changing clear width of flow. This is represented by K_2 value at table 4 and also taken into account in the calculation. It also can be seen from the values of table 7 to 9, when the flow angle is 30° , the calculated scour depths for square nose, round nose and sharp nose are larger than the cylindrical pier and further increases with the increase of the flow angle.

5. Conclusion

In a natural river, it is always possible to change the flow direction due to erosion or deposition of sediments. Therefore any bridge pier constructed in a natural river could experience angular flow attack. Hence it is not recommended to evaluate maximum scour depth for a bridge pier by considering the flow as axial. It is clearer from the analysis results optimum pier section for the pier is circular section, since it has a minimum scour depth with considering all possible scenarios on scour at bridge pier. However if the engineer need to design bridge with different shapes of pier, it is necessary to consider the scour for angular flow conditions. If the pier shape is not a constrain for the design of a bridge, it is economical and safer to design the bridge with circular piers.

References

1. F. Huber, "Update: Bridge Scour," Civil Engineering, ASCE, Vol. 61, No. 9, pp. 62-63, September 1991.
2. B.W. Melville, and A.J. Sutherland, "Design method for local scour at bridge piers," American Society of Civil Engineering, Journal of the Hydraulics Division, Vol. 114, No. 10, pp. 1210-1225, 1988.
3. J. Chabert and P. Engeldinger, "Erosion at piers bottom," National Hydraulic Laboratory Report, France, 1956.
4. E.M. Laursen and A. Toch, "Scour around bridge piers and abutments," Iowa City, IA, Iowa Highway Research Board, Bulletin No. 4, p. 60, 1956.
5. R.J. Garde, K. Subramanya and K.D. Nambudripad., "Study of scour around spur-dikes," American Society of Civil Engineering, Journal of the Hydraulics Division, Vol. 87, No. HY6, pp. 23-37, 1961.
6. R.J. Garde and A.S. Paintal, "Velocity Distribution in Alluvial Channels," Le Houille Blanche, No.4, 1964.
7. R.J. Garde, "Total Sediment Transport in Alluvial Channels," PhD Thesis, Colorado State, University, Fort Collins (USA), 1959.
8. R.J. Garde and U.C. Kothyari "Scour around bridge pier," J. Ind. Nat. Acad. New Delhi, Vol.64, pp. 569-580, 1998.
9. U.C. Kothyari, "Bridge pier scour in gravel - cobble and cohesive bed rivers," Report submitted to the IRC- sub- committee to receive the aspects of scour around bridge foundations, 2003.
10. U.C. Kothyari, "Frequency distribution of river - bed materials," J.Sedimentology, Vol. 42, pp.283-291, 1995.
11. A.J. Raudkivi, "Effect of bed material size on scour," 4th international conference applied numerical modeling Taiwan, 1984.
12. U.S. Department of Transportation, "Recording and Coding Guide for the Structure Inventory and Appraisal of the Nation's Bridges," Federal Highway Administration, Washington, D.C, 1988.
13. U.S. Department of Transportation, "Interim Procedures for Evaluating Scour at Bridges," Federal Highway Administration, Washington, D.C, 1988.
14. U.S. Army Corps of Engineers, "Scour and Deposition in Rivers and Reservoirs," User's Manual, HEC-6, Hydrologic Engineering Center, Davis, CA, 1991.
15. E.M. Laursen, "Scour at Bridge Crossings," Journal Hydraulic Division, American Society of Civil Engineers, Vol. 39, No. HY 3, 1960.
16. E.M. Laursen, "An Analysis of Relief Bridge Scour," Journal Hydraulic Division, American Society of Civil Engineers, Vol. 92, No. HY 3, 1963.
17. A.J. Raudkivi and R. Ettema, "Effect of Sediment Gradation on Clear-Water Scour," American Society of Civil Engineers, Vol. 103, No. HY 10, 1977.
18. A.J Raudkivi, "Functional Trends of Scour at Bridge Piers," American Society of Civil Engineers, Journal Hydraulic Division, Vol 112, No.1, 1986.
19. B.W. Melville and A.J Sutherland, "Design Method for Local Scour at Bridge Piers," American Society of Civil Engineers, Journal Hydraulic Division, Vol. 114, No. 10, October.1988.



20. E.V. Richardson, D.B. Simons, and W.L. Haushild, "*Boundary Form and Resistance to Flow in Alluvial Channels*," Bulletin of International Association of Hydrologic Science, Belgium, 1962.
21. C.R. Neill, "*Note on Initial Movement of Coarse Uniform Bed Material*," Journal of Hydraulic Research, Vol. 17, No. 2, pp. 247-249, 1968.
22. R.E. Ettema "*Scour at bridge piers*," Report No. 236, School of Engineering. The University. of Auckland, New Zealand, 1980.

SECTION II



Trial Introduction of a Bus Lane on A02: A Post-Mortem

K. S. Weerasekera

Abstract: Along Colombo - Galle road (A02) in Sri Lanka (one of the main radial arterial roads connecting southern Sri Lanka with the Colombo capital) few years back due to heavy in flow of morning traffic towards Colombo, a transit lane for public and private buses was introduced (kerb side lane was totally dedicated to buses only, as a solution to address this heavy inflow of traffic to Colombo). This kerb side transit lane was introduced between Dehiwala and Bambalapitiya on trial basis with the assistance of the Colombo city traffic police. Although the new introduction seem to be successful initially, but with passage of time due to unauthorized vehicles getting to the transit lane for their benefit and also buses not sticking to transit lane, led to a drop of efficiency in the transit lane and finally the trial effort was completely given up.

Through this study it is expected to look at the problem from queuing theory point of view and an attempt is made to find out where the failures took place and expect to bring in positive suggestions and corrective measures.

Keywords: Bus Lanes, Transit Lanes, Queuing Theory Models, Queuing Theory.

01. Introduction

The kerb side transit lane for buses (both public and private) was introduced along A02 (Colombo – Galle road) from Dehiwala via Wellawatta to Bambalapitiya on experimental basis for a short period of time around two weeks. During weekdays the roadway under consideration was made a 'clearway' & the operation time was limited from 7:00am to 9:00pm to cover the peak flows. During the operation period the bus lane operation was monitored, and vehicles traveling along both lanes were separately counted. The transit lane was dedicated exclusively for buses and passenger carrying vans only. The purpose of the transit lane was to segregate transit traffic from other vehicles and to prevent interference of one from the other. Transit lanes are designed to provide faster and more reliable public transport for commuters in an attempt to increase support and to reduce the number of cars and other vehicles on the main road system during peak hours.

2. Application of Queuing theory on Bus Lanes

An attempt was made to apply queuing theory to study the operation of transit lanes (1) when smoothly operating under the strict supervision of police and, (2) when intruders violate the

transit movement when police supervision was relaxed.

Figure 1 indicates lane operation before the transition lane was introduced (i.e. when all traffic towards Colombo was taken through the two lanes available towards Colombo direction).

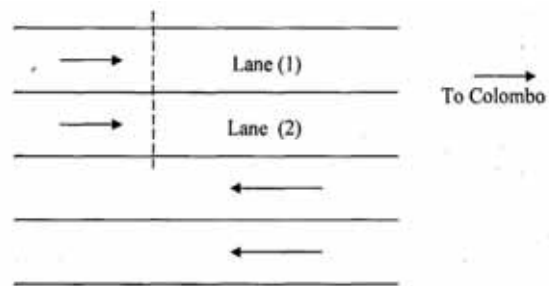


Figure 1 - General arrangement without transit lanes [M/M/2 queuing model]

Figure 2 indicates when transition lane was introduced and with supervision of police when in smooth operation.

Eng. (Prof.) K. S. Weerasekera, BSc Eng (Moratuwa), MEngSc (UNSW), PhD (UNSW), FIE (Sri Lanka), CEng, IntPE(SL), MIE (Aust), CPEng, MIHT (UK), MASCE, Professor in Civil Engineering, Department of Civil Engineering, The Open University of Sri Lanka.



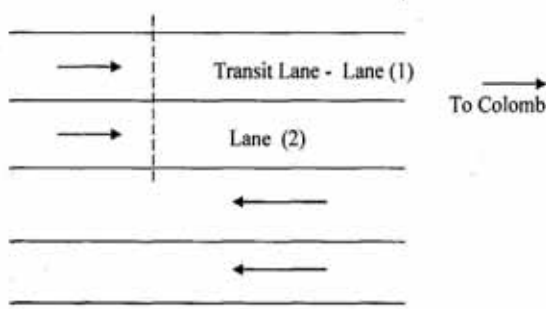


Figure 2 - With-flow transit lane on smooth operation [2(M/M/1) model]

3. Methodology

When applying queuing theory to the above two cases, the arrival rate of vehicles can be assumed to be a Poisson distribution for a random arrival of traffic (Adams, 1936). Pignataro (1973) further strengthened this assumption with further examples. If a roadside observer is noting the time difference between two consecutive vehicles passes (i.e. headways) in each lane, it can be considered as the service time of each vehicle in that lane. Hence the service time of each lane can be obtained.

Before Lane (1) is converted to a transition lane, total flow of traffic during peak hour towards Colombo was noted to be 2200 veh/hr (on both lanes). Total of busses and passenger carrying vans on both lanes was noted to be 450 veh/hr (i.e. 20% of total flow)

The study was conducted as two separate cases.

Case (a) – General arrangement without transit lane arrangement

Case (b) – With flow transit lane operation.

4. Analysis & Results

Case (a) - General arrangement without transit lanes

The traffic is assumed to be equally distributed between the two lanes. This is similar to a M/M/2 type queuing model with 2 service facilities.

The model parameters are as follows:

The arrival pattern is a Poisson distribution (Adams 1936; Pignataro 1973). It was also observed that the cumulative flow curve was as indicated in Figure 3.

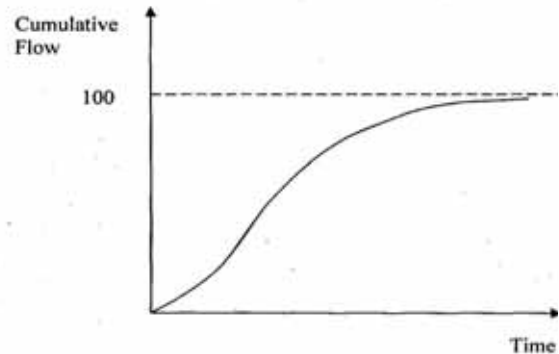
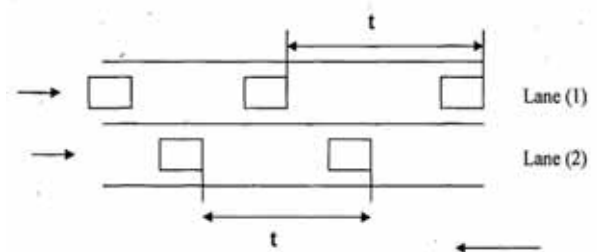


Figure 3 - Cumulative arrival flow

If the flow is being observed from a roadside fixed point, the average rate of service of a lane (μ) can be considered as the reciprocal of average headway between two consecutive vehicles.



t – average headway of both lanes

Figure 4 - The average headway of both lanes (when without transit lanes)

Flow in lane (1) = Flow in lane (2) = q
 $q = 2200 / (2 \times 3600) = 0.305 \text{ veh/sec/lane}$
 Average headway (i.e. average service time) = $1/q = 1/0.305 = 3.27 \text{ secs}$
 Service rate of a lane = $\mu = 1 / (\text{Average headway}) = 0.305 \text{ veh/sec/lane}$

Case (b) - With-flow transit lane on operation

When transit lane is operating, 450 vehicles traveled on transit lane and balance will take the other lane. If assumed that no transit lane

violators (i.e. the ideal condition). This will behave as two M/M/1 models.

$$\text{Flow in lane (1)} = 450/3600 = 0.125 \text{ veh/sec/lane}$$

$$\text{Flow in lane (2)} = 1750/3600 = 0.486 \text{ veh/sec/lane}$$

Hence,

$$\text{Service rate of lane (1)} = \mu_1 = 0.125 \text{ veh/sec/lane}$$

$$\text{Service rate of lane (2)} = \mu_2 = 0.486 \text{ veh/sec/lane}$$

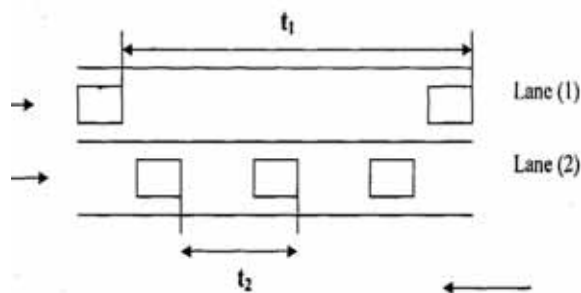


Figure 5 - The average headway of lane (1) & lane (2) [with flow transit lane on operation]

t_1 = average headway in lane (1)

t_2 = average headway in lane (2)

Service time of lane (1); $t_1 = 1/0.125 = 8.0$ secs

Service time of lane (2); $t_2 = 1/0.486 = 2.057$ secs

$$t_1 > t_2$$

5. Conclusions

Hence now lane (1) has a higher service time and lane (2) has a lower service time, this in reverse will drop the service rate (μ_1) of lane (1) and increase the pressure on the service rate of lane (2). If the saturation of lane (2) has occurred, then the transit lane operation may bring down the total vehicle throughput on the road. But though the number of vehicles in transit lane has dropped, due to the high occupancy rate in vehicles occupying this lane, there will be an overall improvement in the total passenger travel time.

Effect due to Transit Lane occupied by banned Vehicles

Breaching of transit lane regulations occur when unauthorized vehicles get on to the transit lane and use for their benefit. Once this happened with relaxing of police monitoring the transit lane discipline, the efficiency of the transit lane dropped.

Wei and Chong (2002); Viegas et al. (2007) have indicated the problem of veering into transit lanes to dodge traffic queues which is often happening when monitoring is relaxed. Shapiro (2008) discusses the role played by monitoring with the help of fixed cameras in maintaining discipline.

In queuing theory, model used for transit lanes shown when operating smoothly as shown in Figure 2, it was shown that the two lanes were behaving as two M/M/1 models. It should be noted that this behaviour will prevail only if there is no mixing of vehicles between the two lanes. If more transit lane breaching is occurring, the model will stop behaving as two separate M/M/1 queues, and neither will behave as M/M/2 model.

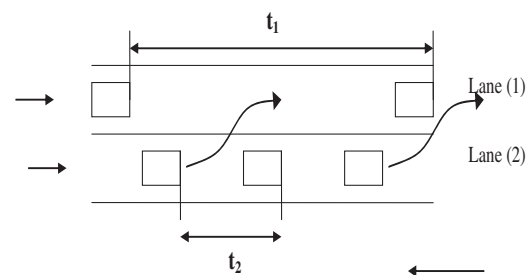


Figure 6 - Breaching of transit lane regulations

When transit lane regulations are violated it can affect the function of the transit lane in following manner.

- Smooth flow in transit lane can get disturbed due to unauthorized lane changing by other vehicles along the transit lane as indicated in Figure 6.
- Vehicle flow in transit lane will increase while decreasing the level of service in the transit lane.
- Average speed in the transit lane will reduce.
- When unauthorized vehicles get on to the smooth flowing transit lane at unexpected times, the well maintained headway between the vehicles in transit lane may get affected, causing harmful influence on the



expected regularity and punctuality of the bus service.

6. Recommendations

Police can enforce the transit lane regulations by stopping the violators and warning them in the initial stage. If it seems that punishment by warning is not severe enough fines can be imposed on the transit lane violators. Police can operate random checking points and catch the transit lane violators in a similar manner to catching the high speed drivers and alcoholic drivers.

References

1. Adams, W. F., "Road Traffic Considered as a Random Series", *Journal of the Institution of Civil Engineers*, Vol. 4, November, 1936, pp. 121-130.
2. Gross, D. and Harris, C. M., *Fundamentals of Queuing Theory*, 2nd Edition, John Wiley & Sons, New York, 1985
3. Pignataro, L. J., *Traffic Engineering, Theory and Practice*, Prentice-Hall, Inc., Englewood Cliffs, New Jersey, 1973
4. Shapiro, J., "City tells Downtown skeptics the Broadway bus lane 'seems' to work", *Downtown Express*, Vol. 21, No. 33, December, 2008, pp. 19-25.
5. Viegas, J. M., Roque, R., Lu, B. and Vieira, J., "The Intermittent Bus Lane System: Demonstration in Lisbon", *86th TRB Annual Meeting* - 2007.
6. Wei, L., Chong, T., "Theory and Practice of Bus Lane Operation in Kunming, 2002, pp. 68-72.

Computer Aided Design of Modern High-Rise Building

G.A.P. Gampathi and P.P.P. Peiris

Abstract: The major cities of Sri Lanka are fast changing with many residential apartment buildings constructed. One of the primary requirements is the provision of car parking for which the lower floors are generally used. The car parks have a certain grid requirement for vertical load carrying members primarily arising due to guidelines specified in Building Regulations. Often, this grid arrangement is not suitable for the residential apartment above. Therefore, it is necessary to introduce a load transfer method at the starting of the apartment floors. This paper describes a complete design of a load transfer plate using finite elements as a solution to a 25 storied reinforced concrete building in Colombo, Sri Lanka which has car parking floors up to 5th storey. Further it is recommended to apply transfer plate concept as a solution to various space requirements and advancements of architectural features in modern high-rise building.

Keywords: Car parking, Grid, Building regulation, Load transfer plate, High-rise building

1. Introduction

When considering the present situation in major cities of the country, land is a scarce resource. So every bit of land is precious and it is used for some important purpose. Thus, high rise apartment buildings are in demand. The current trend is to use the entire land for the structure and provide several parking floors within the building rather than providing parking outside [5]. The suitable column grid of an apartment floor will never match that of a parking floor which gives rise to the issue of connecting the two sets of columns together. There are several ways of connecting the two floors. Either girders or plates can be used as the transfer system. The selection of the system depends on the architectural features of the apartments and the client requirements. The project which I undertook was a 25 storeys reinforced concrete building, located in No.61, Green Path, Colombo 06, Sri Lanka. The proposed building will be used as a residential building with car parking up to 5th storey level and floor area at each floor level is 788 m². In this project, at the structural design stage, client requested to change the transfer beams and column grids at 6th storey since it was affecting the internal view of the residential apartment but the client also requested to keep the external views as per the architectural drawings. Therefore structural engineers had to face a challenge to find a suitable structural system for the building.

2. Objectives

The objective of this project is to introduce a thick plate for transferring loads from residential floors to columns continue from the car parking floors as a solution to safeguard the internal and external architectural requirement of residential apartments. Determination of a proper way to model a thick transfer plate in finite elements is also looked at in addition to obtaining the design parameters of the transfer plate from the finite element model.

3. Methodology

First a typical apartment layout and a parking layout were selected that satisfied the building and parking regulations. Foundation system was selected as bored piles with pile caps to satisfy existing soil condition at site.

The final structural system was selected as columns, beams and slabs up to 5th floor, load transfer plate at 6th floor level and wall and flat slabs from 6th floor to roof. The analysis was done based on a finite element model in SAP2000 with seven load combinations. Lateral stability was measured in terms of fundamental period of vibration and deflection for wind loads. The wind load analysis was carried out according to CP3: chapter V as it is widely used in Sri Lanka.

*Eng. G A P Gampathi- M.Eng (NUS), B.Sc (Hons), AMIE(Sri Lanka), Senior Engineer Sanken Lanka Pvt. Ltd
Eng. P P P Peiris – PG Dip (Moratuwa), B.Sc (Hons), C.Eng. MIE(Sri Lanka), Manager Design Sanken Lanka Pvt. Ltd.*



4. Car parking regulations

It is necessary to allow space for vehicle turning circles, parking stalls, ramps, driveways etc... when arranging a parking floor. This must be done satisfying the parking regulations in Sri Lanka. As a result, the vertical load carrying members should have a certain grid requirement [6]. Columns are the most suitable elements to transfer vertical loads and the dimensions of a suitable column grid are largely dependent on the parking regulations. This study is limited to relevant regulations for standard vehicle type, such as car equivalent, two and three wheelers. More evidently, multi-storey car parks in high rise apartment buildings are designed for car equivalent, two and three wheelers.

Table 1: Minimum plan dimensions of Parking Stalls

Vehicle Type	Stall width (m)	Stall length (m)
Standard (Car equivalent, also to be used for two and three wheelers)	2.4	4.8

Table 2: Minimum width of Aisles

Parking Angle (Degree's)	One way traffic one sided bays (m)	One way traffic two sided bays (m)	Two-way traffic (m)
00° Parallel	3.6	3.6	6.0
30° Angle	3.6	4.2	6.0
45° Angle	4.2	4.8	6.2
60° Angle	4.8	4.8	6.4
90° Angle	6.0	6.0	6.0

Table 3: Minimum inner and outer Turning Radius

	Passenger Car
Inner turning radius (m)	7.3
Outer turning radius (m)	4.7

5. The need of different grids for the proposed apartment building and solution with transfer plate

The proposed residential apartment building at green path, Colombo 7, Sri Lanka has 6 car parking floors with one at basement level. The other floors from 6th storey level to 25th storey level are residential apartment floors. Each of these residential floors has six apartments with advanced architectural features. Therefore to cater the different space allocation needs of the apartment floors and the parking floors, primarily arising due to building regulations and traffic regulations, it was necessary to have different grids in the same building. As a result of this situation, regular column grid has been changed at the sixth storey level with a transfer plate and concrete walls.

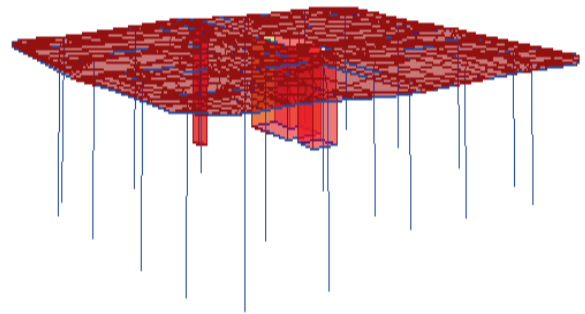


Figure 01: Column layout below the transfer plate

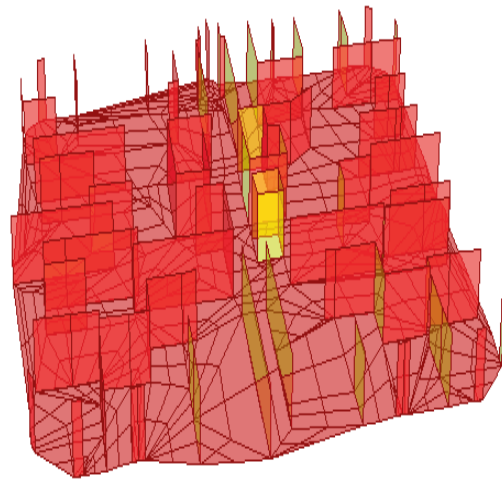


Figure 02: Wall layout above transfer plate

6. Transfer plate – SAP2000 model

It is necessary to select a correct finite element to represent the behavior of the transfer plate; in this case a shell element was selected to represent the transfer plate. However, there are

certain issues when using shell elements. The height of the stories above and below the transfer level must be increased to maintain the overall height of the structure. This is because of transfer plate element thickness does not add to the height of the building at the common connecting point of top and bottom column elements and transfer plate elements [8]. Another concern of using shell elements for this situation is that of Shearing deformations. Shearing deformations tend to be important when the thickness of the element is greater than about one –tenth to one-fifth of the span. They can also be quite significant in the vicinity of bending-stress concentrations, such as near sudden changes in thickness or support condition, and near holes or re-entrant corners. Thus, shearing deformations had been taken into account by selecting shell element properties as thick plate. This formulation includes the effects of transverse shearing deformation [5]. However, there are important aspects that a design engineer must be aware of in this situation. All shell elements must be properly connected to adjoining elements to have proper connectivity and these elements should be connected with different column grids while maintaining connectivity and keeping orientation.

7.0 Meshing for better results

In any finite element model the finer the mesh more accurate are the results. This is particularly important in this situation as concentrations of stress are most likely around columns that are transferred. Further more, as explained earlier the use of the thick-plate formulation implies that the shell elements are more sensitive to large aspect ratios. If a coarse mesh is to be used, elements with large aspect ratios are most likely particularly in the vicinity of the loads (columns that are transferred).

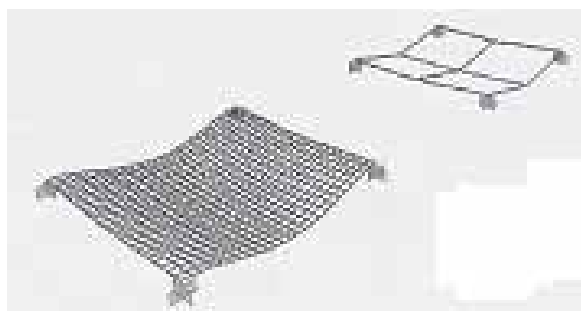


Figure 03: The behavior of a fine mesh and a coarse mesh

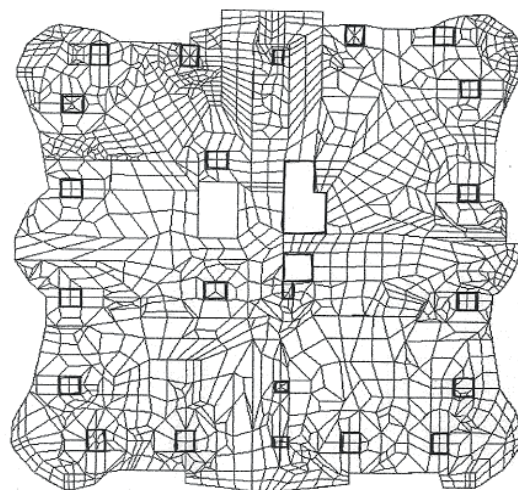


Figure 04: Transfer plate model

8. Complete Model – SAP2000

The complete modeling was carried out after selecting proper finite elements to represent all the structural members, finalizing initial member sizes and support conditions. Support conditions were selected as pin to transfer loads from column to pile foundation. In addition to the selection of element type for transfer plate as thick plate shell element, the other element types were selected to represent column, beam, slab and wall. Column and beam were represented by frame elements while slab and wall were represented by shell elements. Modeling was carried out step by step. First pin supports were introduced at column positions with ground beams and slabs at basement location and then as to the conventional beam, slab and column system; all the columns, beams, lift walls, slabs, ramps and stair cases were modeled up to the 6th storey level. At the second stage of modeling transfer plate was modeled by connecting column grids and wall grids rising upward from transfer plate. After introducing suitable wall grids for apartment walls at 6th storey, the typical 7th storey was modeled with a flat slab and repeated up to roof level with stair cases and lift walls. A few walls and lift walls were extended from the roof level to support for lift machine room and water tank. The building model was completed after modeling the lift machine room and the water tank.



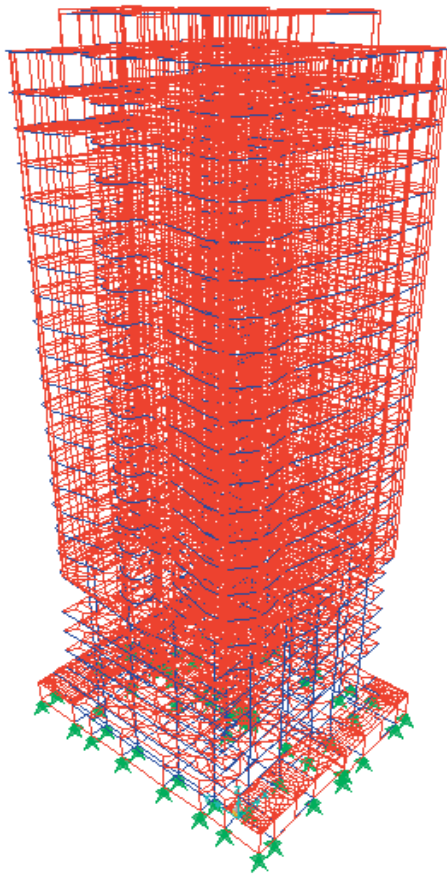


Figure 05: Complete 3 D Model

9. Loading :

Dead and Imposed loadings on building were calculated by using BS 6399 Part I: 1984, British standard of design loadings for buildings and Wind loadings were calculated from CP3: Chapter V: Part 2: 1972, code of basic data for the design of buildings. Considering the construction difficulties with using deferent concrete grades for structural elements; grade 40 concrete ($f_{cu} = 40 \text{ N/mm}^2$) was selected for all structural members. Further, in the analysis part seven different load combinations were introduced and analyses were carried out for all structural members to have greater safety.

10. Analysis:

Analyses were carried out for the following seven different load cases; in addition to considering wind load from two directions.

Load Case 1 - All span with maximum load (1.4 DL + 1.6 IL)

Load Case 2 – Span loaded with maximum / minimum / maximum load combination

Load Case 3 - Span loaded with minimum /

maximum / minimum load combination

Load Case 4 – 1.4 DL + 1.4 WL

Load Case 5 – 1.2 DL + 1.2 IL + 1.2 WL

Load Case 6 – 1.4 DL – 1.4 WL

Load Case 7 - 1.2 DL + 1.2 IL - 1.2 WL

Fine meshes were used for typical apartment floors and transfer plate to study the effect of meshing at load transfer locations. The mesh generation and the stress contours for S_{11} (Stresses in direction 11 for Load case 1) at transfer plate are shown below for two models.

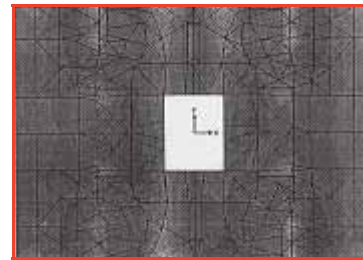


Figure 06: Mesh generation and the stress contours for Model-1

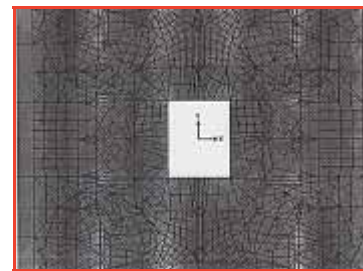


Figure 07: Mesh generation and the stress contours for Model-2

11. Results:

11.1 Lateral Stability Analysis

Table 4: Deflection and fundamental period of vibration

Parameter	Value
Fundamental period of vibration	2.00 sec.
Maximum deflection for wind loads	24 mm
Maximum vertical deflection of transfer plate	10 mm
Maximum lateral deflection of transfer plate	3.5 mm

From these results it is seen that there is an important aspect of low value vibration period. Based on rule of thumb, the acceptable value is about 2.5 sec for a 25 storey building, but in this case it is 2.00 sec. It seems that the apartment above the transfer plate contributes much more than the structure below the transfer plate due to high stiffness of the building up to the transfer plate level. It also can be seen that lateral deflections of the transfer plate level is only 3.5mm but at the tip of the building is 24mm. Therefore, it is clear that lateral deflections of the transfer plate and below are at a minimum. Effectively, the apartment structure behaves as it is supported on a rigid foundation.

Designing the transfer plate

Table 5: Critical stress in the transfer plate

Maximum stress N/mm ²	Top surface	Bottom surface
Compression (S ₁₁)	13.74	26.32
Tensile (S ₁₁)	24.32	10.82
Compression (S ₂₂)	8.37	17.20
Tensile (S ₂₂)	18.27	9.45

* S₁₁ – Stress in direction 11

S₂₂ – Stress in direction 22

M₁₁ – Moment in direction 11

M₂₂ – Moment in direction 22

It can be seen from the analysis results that the highest stresses are located at around the column and do not progress for lengths more than 1-1.5m (Figure: 07). The design steel can be calculated either based on stress S₁₁ and S₂₂ or directly using M₁₁ and M₂₂.

12. Conclusion

It can be concluded that the transfer plates can be used effectively as outriggers in apartment buildings. It will allow changing column grids above to project architectural features within apartments. A proper finite element model gives the required design parameters for the transfer plate itself and parameters regarding the lateral behavior of the structures. Once a thick plate is used, the effects of the floors below the transfer level have no considerable impact on the lateral

behavior of the overall building. It will act as a rigid component without much deflection.

References

1. Allen, A.H., "Reinforced concrete design to BS 8110". Spon Architecture, India, pp 193-202.
2. British Standards, BS 6399 – Part I, (1984), "Design loading for buildings".
3. British Standards, BS 8110 – Part I and Part II, (1985), "Structural use of concrete".
4. CP3: Chapter V: Part 2, (1972), "Code of basic data for the design of buildings – wind loading".
5. Jayasinghe, M.R., Balasuriya, S.S. (2007), "The influence of transfer plates on the lateral behavior of apartment buildings", IESL Transactions.
6. Ministry of Housing and Construction, (1980), "Design of buildings for high wind Sri Lank", July, pp 18-40.
7. Mosley, W.H., Bungey, J.H. "Reinforced concrete design", Macmillan press Ltd, pp 192-230.
8. SAP2000, "Basic Analysis reference manual, linear and nonlinear static and dynamic analysis and design of three-dimensional structures", Computers and Structures, Inc, Berkeley, California, USA.

